Gravitational lensing

Philippe Jetzer

Institute of Theoretical Physics
University of Zürich, Winterthurerstrasse 190, CH-8057 Zürich

February 11, 2005

Contents

Contents **v**

1 Introduction **1**
1.1 Historical remarks 2

2 Lens equation **5**
2.1 Point-like lenses 5
2.2 Thin lens approximation 7
2.3 Lens equation 8
2.4 Remarks on the lens equation 10
2.4.1 Classification ordinary images 14

3 Simple lens models **16**
3.1 Axially symmetric lenses 16
3.1.1 Tangential and radial critical curves 17
3.1.2 Einstein radius 18
3.2 Schwarzschild lens 19
3.3 Singular isothermal sphere 21
3.4 Generalization of the singular isothermal sphere 22
3.5 Extended source 23
3.6 Two point-mass lens 24

4 Galactic microlensing **25**
4.1 Introduction 25
4.1.1 Microlensing probability 27
4.1.2 Microlensing towards the LMC 30
4.1.3 Microlensing towards other targets 33

5 The lens equation in cosmology **35**
5.1 Hubble constant from time delays 37

6 Galaxy clusters as lenses **40**
6.1 Weak lensing 42
6.2 Comparison with results from X–ray observations 45

References **48**

Chapter 1

Introduction

Gravitational lensing - i.e. light deflection by gravity - has become in the last few years one of the most important fields in present day astronomy. The enormous activity in this area has mainly been driven by the considerable improvements of the observational capabilities. Due to the new wide-field cameras and telescopes which are already in place or will become operational in the near future the rate and the quality of the lensing data will increase dramatically. Gravitational lensing is independent of the nature and the physical state of the deflecting mass, therefore, it is perfectly suited to study dark matter at all scales.

Indeed, the determination of the amount and the nature of matter present in the Universe is an important problem for contemporary astrophysics and cosmology. This knowledge is directly related to the question of the fate of the Universe: will it expand forever or, after a phase of expansion, collapse again. There are several astrophysical observations which indicate that most of the matter present in the Universe is actually dark and, therefore, cannot be detected using telescopes or radiotelescopes. The most recent studies seem to suggest that the total matter density is only about 30% of the "closure density" of the Universe: the amount of mass that would make the Universe balance between expanding forever and collapsing. Measurements based on high-redshift supernovae suggest that there is also a non-vanishing cosmological constant, such that the sum of matter density and cosmological constant implies a flat Universe [1].

Important evidence for the existence of large quantities of dark matter comes from the measured rotation curves of several hundreds of spiral galaxies [2], which imply the presence of a huge dark halo in which these galaxies are embedded. Typically, a galaxy including its halo contains ~ 10 times more dark than luminous matter, the latter being in the form of stars and gas. There are also clear indications for the presence of important quantities of dark matter on larger scales, in particular in clusters of galaxies. This was first pointed out in 1933 by Zwicky [3]. Since then,

much effort has been put into the search for dark matter, the nature of which is still largely unknown.

The field of gravitational lensing is growing very rapidly and almost daily there are new results, therefore it will not be possible to give here a complete and exhaustive review of the field and of all the results achieved so far. The present lecture notes are more intended as a way to rapidly get the main ideas and tools of lensing, which will then enable to read the original literature. For more details see the book of Schneider et al. [4] as well as some reviews [5, 6, 7] and the references therein.

Before beginning with the theory of lensing lets briefly give some historical remarks on the developpment of the field.

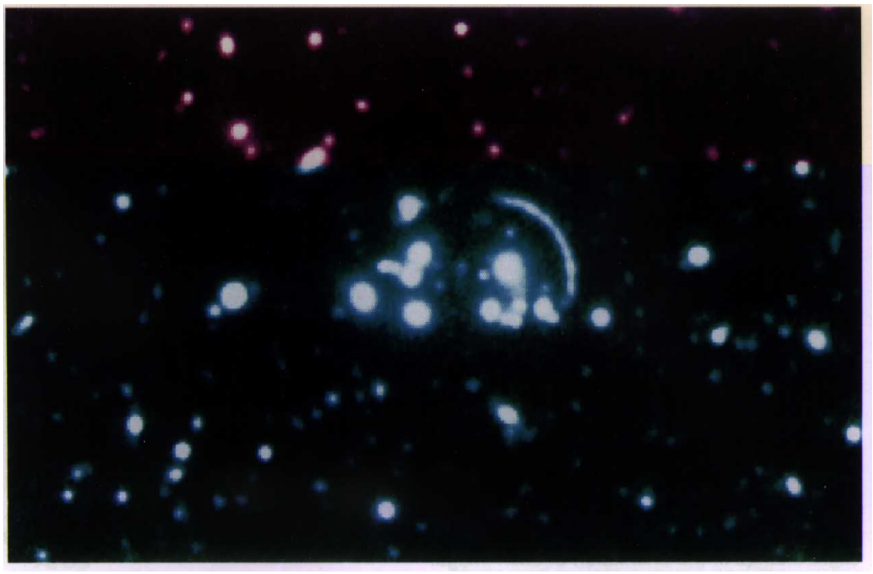

Figure 1.1. Giant arc in Cl2244-02 (image from CFHT). The lensing cluster is at $z = 0.329$ and the source of the arc is a very distant field galaxy at $z = 2.238$. (Courtesy of G. Soucail, Obs. Midi–Pyrénées, ESO Messenger 69, September 1992.)

1.1 Historical remarks

Nowadays we know that the light propagation in a gravitational field has to be described using the theory of general relativity by Einstein formulated in 1915. However, long before it was argued that gravity might influence the behaviour of light (for a historical account, see for instance the book

by Schneider et al. [4]). Indeed, already Newton in the first edition of his book on optics appeared in 1704 discussed the possibility that celestial bodies could deflect the light trajectory. In 1804 the astronomer Soldner published a paper in which he computed the error induced by the light deflection on the determination of the position of stars. To that purpose he used the Newtonian theory of gravity assuming that the light is made of particles. He also estimated that a light ray which just grazes the surface of the sun would be deflected by a value of only 0.85 arc seconds. Within general relativity this value is about twice as much, more precisely 1.75 arc seconds. The first measurement of this effect has been made during the solar eclipse of 29 mai 1919 and confirmed the value predicted by general relativity [8].

In 1936 Einstein published a short paper in Science in which he computed the light deflection of light coming from a distant star by the gravitational field of another star [9]. He mentioned that if the source and the lens are perfectly aligned the image would be a ring. If instead the alignement is not perfect one would see two images with, however, a very small separation angle. Einstein also wrote: "Of course, there is no hope of observing this phenomenon". Actually, it has been found recently that Einstein made most of the calculations presented in that paper already in 1912 as can be seen on some pages of his notebook [10]. The recent developments of microlensing show that Einstein's conclusion, although understandable at that time, was too pessimistic. Indeed, the formulae developed by Einstein in his 1936 paper are still the basis for the description of gravitational lensing.

In the following year 1937 the swiss astronomer Zwicky wrote two short articles in Physical Review suggesting to consider galaxies as sources and lenses rather than stars as mentioned by Einstein [11]. He came to the conclusion that such a configuration would have much higher chances to be seen, since the typical mass of a galaxy is several billion times higher than the mass of as single star. He argued that such configurations must almost certainly be seen. Moreover, he gave also a list of possible applications among which the possibility to better determine the total mass of galaxies, including their dark matter content.

The first gravitational lens has been discovered in 1979, when spectra were obtained of two point-like quasars which lie only about 6 arc seconds away. The spectra showed that both objects have the same redshift and are thus at the same distance. Later on also the galaxy acting as lens has been found, making it clear that the two objects are the images of the same quasar, which is lensed. Since then many other examples have been found, and in 1986 the first lensing case with a galaxy acting as source was discovered. The galaxy appears then distorted as one or more arcs. Many such systems have since then be discovered, some thanks to the Hubble space telescope. In 1979, Chang and Refsdal [12], and in 1981, Gott [13]

noted that even though a point mass in a halo of a distant galaxy would create an unresolvable double image of a background quasar, the time variation of the combined brightness of the two images could be observed. In this way, the effect of non-luminous matter in the form of compact objects could be observed. The term *microlensing* was proposed by Paczyński [14] to describe gravitational lensing which can be detected by measuring the intensity variation of a macro-image made up of any number of unresolved micro-images.

In 1993 the first galactic microlensing events were observed, in which the source is a star in the Large Magellanic Cloud and the galactic bulge. In the former case the lens is a compact object probably located in the galactic halo, whereas in the later case the lens is a low mass star in the galactic disk or in the bulge itself.

Chapter 2

Lens equation

2.1 Point-like lenses

The propagation of light in a curved space-time is in general a complicated problem, however, for almost all relevant applications of gravitational lensing one can assume that the geometry of the universe is described in good approximation by the Friedmann-Lemaître-Robertson-Walker metric. The inhomogeneities in the metric can be considered as local perturbations. Thus the trajectory of the light coming from a distant source can be divided into three distinct pieces. In the first one the light coming from a distant source propagates in a flat unperturbed space-time, nearby the lens the trajectory gets modified due to the gravitational potential of the lens and afterwards in the third piece the light travels again in an unperturbed space-time till it gets to the observer. The region around the lens can be described by a flat Minkowskian space-time with small perturbations induced by the gravitational potential of the lens. This approximation is valid as long as the Newtonian potential Φ is small, which means $\mid \Phi \mid \ll c^2$ (c being the velocity of light), and if the peculiar velocity v of the lens is negligible as compared to c. These conditions are almost always fulfilled in all cases of interests for the astrophysical applications. An exception, for instance, is when the light rays get close to a black hole. We will not discuss such cases in the following.

With the above simplifying assumptions we can describe the light propagation nearby the lens in a flat space-time with a perturbation due to the gravitational potential of the lens described in first order post-Newtonian approximation. The effect of the space-time curvature on the light trajectory can be described as an effective refraction index, given by

$$n = 1 - \frac{2}{c^2}\Phi = 1 + \frac{2}{c^2} \mid \Phi \mid \ . \tag{2.1}$$

The Newtonian potential is negative and vanishes asymptotically. As in geometrical optics a refraction index $n > 1$ means that the light travels

with a speed which is less as compared with its speed in the vacuum. Thus the effective speed of light in a gravitational field is given by

$$v = \frac{c}{n} \simeq c - \frac{2}{c} \mid \Phi \mid \ . \tag{2.2}$$

Since the effective speed of light is less in a gravitational field, the travel time gets longer as compared to the propagation in the empty space. The total time delay Δt is obtained by integrating along the light trajectory from the source till the observer, as follows

$$\Delta t = \int_{source}^{observer} \frac{2}{c^3} \mid \Phi \mid dl \ . \tag{2.3}$$

This is also called the Shapiro delay.

The deflection angle for the light rays which go through a gravitational field is given by the integration of the gradient component of n perpendicular to the trajectory itself

$$\vec{\alpha} = -\int \vec{\nabla}_\perp n \ dl = \frac{2}{c^2} \int \vec{\nabla}_\perp \Phi \ dl \ . \tag{2.4}$$

For all astrophysical applications of interest the deflection angle is always extremely small, so that the computation can be substantially simplified by integrating $\vec{\nabla}_\perp n$ along an unperturbed path, rather than the effective perturbed path. The so induced error is of higher order and thus negligible.

As an example lets consider the deflection angle of a point-like lens of mass M. Its Newtonian potential is given by

$$\Phi(b, z) = -\frac{GM}{(b^2 + z^2)^{1/2}} \ , \tag{2.5}$$

where b is the impact parameter of the unperturbed light ray and z denotes the position along the unperturbed path as measured from the point of minimal distance from the lens. This way we get

$$\vec{\nabla}_\perp \Phi(b, z) = \frac{GM \ \vec{b}}{(b^2 + z^2)^{3/2}} \ , \tag{2.6}$$

where $\vec{b}$ is orthogonal to the unperturbed light trajectory and is directed towards the point-like lens. Inserting eq.(2.6) in eq.(2.4) we find for the the deflection angle

$$\vec{\alpha} = \frac{2}{c^2} \int \vec{\nabla}_\perp \Phi \ dz = \frac{4GM}{c^2 b} \ \frac{\vec{b}}{b} \ . \tag{2.7}$$

The Schwarzschild radius for a body of mass M is given by

$$R_S = \frac{2GM}{c^2} \ , \tag{2.8}$$

thus the absolute value of the deflection angle can also be written as $\alpha = 2R_S/b$. For the Sun the Schwarzschild radius is 2.95 km, whereas its physical radius is 6.96×10^5 km. Therefore, a light ray which just grazes the solar surface is deflected by an angle corresponding to $1.7''$.

2.2 Thin lens approximation

From the above considerations one sees that the main contribution to the light deflection comes from the region $\Delta z \sim \pm b$ around the lens. Tipically, Δz is much smaller than the distance between the observer and the lens and the lens and the source, respectively. The lens can thus be assumed to be thin as compared to the full length of the light trajectory. Thus one considers the mass of the lens, for instance a galaxy cluster, projected on a plane perpendicular to the line of sight (between the observer and the lens) and going through the center of the lens. This plane is usually referred to as the lens plane, and similarly one can define the source plane. The projection of the lens mass on the lens plane is obtained by integrating the mass density ρ along the direction perpendicular to the lens plane

$$\Sigma(\vec{\xi}\,) = \int \rho(\vec{\xi}, z)\; dz \;, \tag{2.9}$$

where $\vec{\xi}$ is a two dimensional vector in the lens plane and z is the distance from the plane. The deflection angle at the point $\vec{\xi}$ is then given by summing over the deflection due to all mass elements in the plane as follows

$$\vec{\alpha} = \frac{4G}{c^2} \int \frac{(\vec{\xi} - \vec{\xi}')\Sigma(\vec{\xi}')}{\mid \vec{\xi} - \vec{\xi}' \mid^2}\; d^2\xi' \;. \tag{2.10}$$

In the general case the deflection angle is described by a two dimensional vector, however in the special case that the lens has circular symmetry one can reduce the problem to a one-dimensional situation. Then the deflection angle is a vector directed towards the center of the symmetry with absolute value given by

$$\alpha = \frac{4GM(\xi)}{c^2\xi} \;, \tag{2.11}$$

where ξ is the distance from the center of the lens and $M(\xi)$ is the total mass inside a radius ξ from the center, defined as

$$M(\xi) = 2\pi \int_0^{\xi} \Sigma(\xi')\; \xi'\; d\xi' \;. \tag{2.12}$$

2.3 Lens equation

The geometry for a typical gravitational lens is given in Figure 2.1 A light ray from a source S (in $\vec{\eta}$) is deflected by the lens by an angle $\vec{\alpha}$ (with impact parameter $|\vec{\xi}|$) and reaches the observer located in O.

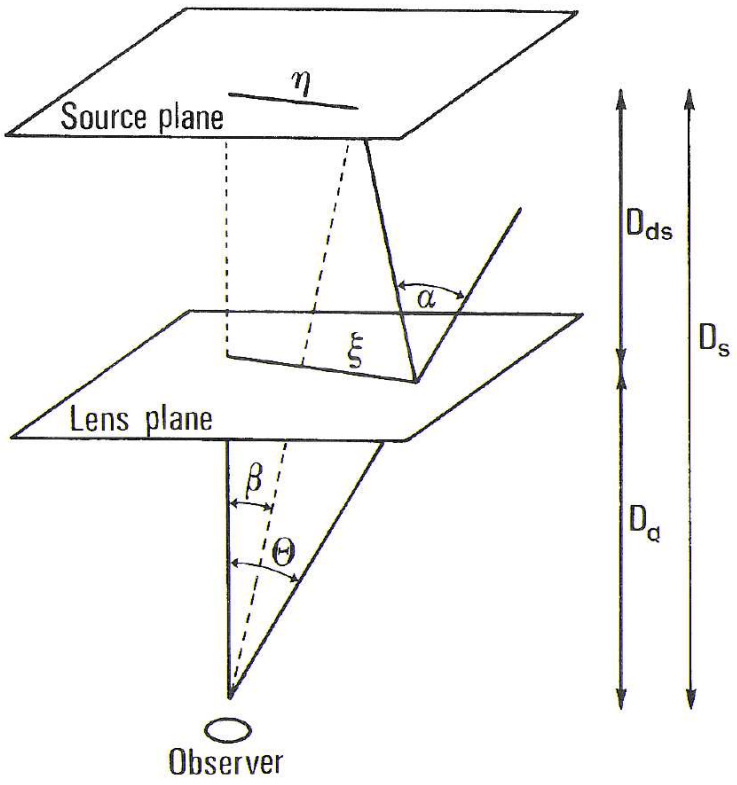

Figure 2.1. Notation for the lens geometry.

The angle between the optical axis (arbitrarily defined) and the true source position is given by $\vec{\beta}$, whereas the angle between the optical axis and the image position is $\vec{\theta}$. The distances between the obser and the lens, the lens and the source, and the observer and the source are, respectively, D_d, D_{ds} and D_s. From Figure 2.1 one can easily derive (assuming small angles) that $\theta D_s = \beta D_s + \alpha D_{ds}$. Thus the positions of the source and the

image are related by the following equation

$$\vec{\beta} = \vec{\theta} - \vec{\alpha}(\vec{\theta}\,)\frac{D_{ds}}{D_s}\ , \tag{2.13}$$

which is called the *lens equation*. It is a non-linear equation so that it is possible to have several images $\vec{\theta}$ corresponding to a single source position $\vec{\beta}$.

The lens equation (2.13) can also be derived using the Fermat principle, which is identical to the classical one in geometrical optics but with the refraction index as defined in eq.(2.1). The light trajectory is then given by the variational principle

$$\delta \int n\ dl = 0\ . \tag{2.14}$$

It express the fact that the light trajectory will be such that the traveling time will be extremal. Lets consider a light ray emitted from the source S at time $t = 0$. It will then proceed straight till it reaches the lens, located at the point I, and where it will be deflected and then proceed again straight to the observer in O. We thus have

$$t = \frac{1}{c}\int \left(1 - \frac{2\phi}{c^2}\right) dl = \frac{l}{c} - \frac{2}{c^3}\int \phi\ dl \tag{2.15}$$

where l is the distance SIO (Euclidean distance). The term containing ϕ has to be integrated along the light trajectory. From Fig. 2.1 we see that

$$\begin{aligned} l &= \sqrt{(\vec{\xi} - \vec{\eta})^2 + D_{ds}^2} + \sqrt{\vec{\xi}^2 + D_d^2} \\ &\simeq D_{ds} + D_d + \frac{1}{2D_{ds}}(\vec{\xi} - \vec{\eta})^2 + \frac{1}{2D_d}\vec{\xi}^2\ , \end{aligned} \tag{2.16}$$

where $\vec{\eta}$ is a two dimensional vector in the source plane If we take $\phi = -GM/\mid \vec{x}\mid$ (corresponding to a point-like lens of mass M) we get

$$\int_S^I \frac{2\phi}{c^3}\ dl = \frac{2GM}{c^3}\left[ln\frac{\mid \vec{\xi}\mid}{2D_{ds}} + \frac{\vec{\xi}\cdot(\vec{\eta} - \vec{\xi}\,)}{\mid \vec{\xi}\mid D_{ds}} + \mathcal{O}\left(\frac{(\vec{\eta} - \vec{\xi}\,)^2}{D_{ds}}\right)\right] \tag{2.17}$$

and similarly for $\int_I^O 2\phi/c^3\ dl$.

Only the logarithmic term is relevant for lensing, since the other ones are of higher order. Moreover, instead of a point-like lens we consider a surface mass density $\Sigma(\vec{\xi}\,)$ (as defined in eq.(2.9)) and so we get for the integral containing the potential term (neglecting higher order contributions)

$$\frac{2}{c^3}\int \phi\ dl = \frac{4G}{c^3}\int d^2\xi'\ \Sigma(\vec{\xi}')\ ln\frac{\mid \vec{\xi} - \vec{\xi}'\mid}{\xi_0}\ , \tag{2.18}$$

where ξ_0 is a characteristic length in the lens plane and the right hand side term is defined up to a constant.

The difference in the arrival time , between the situation which takes into account the light deflection due to the lens and without the lens, is obtained by summing eq.(2.16) to eq.(2.18) and by subtracting the travel time without deflection from S to O. This way one gets

$$c\Delta t = \hat{\phi}(\vec{\xi}, \vec{\eta}) + const. \ , \tag{2.19}$$

where $\hat{\phi}$ is the *Fermat potential* defined as

$$\hat{\phi}(\vec{\xi}, \vec{\eta}) = \frac{D_d D_s}{2D_{ds}} \left(\frac{\vec{\xi}}{D_d} - \frac{\vec{\eta}}{D_s} \right)^2 - \hat{\psi}(\vec{\xi}\,) \tag{2.20}$$

and

$$\hat{\psi}(\vec{\xi}) = \frac{4G}{c^2} \int d^2\xi' \ \Sigma(\vec{\xi'}) \ ln \left(\frac{\mid \vec{\xi} - \vec{\xi'} \mid}{\xi_0} \right) \tag{2.21}$$

is the *deflection potential*, which does not depend on $\vec{\eta}$. The Fermat principle can thus be written as $\frac{d\Delta t}{d\vec{\xi}} = 0$, and inserting eq.(2.19) one gets again the lens equation

$$\vec{\eta} = \frac{D_s}{D_d}\vec{\xi} - D_{ds} \ \vec{\alpha}(\vec{\xi}\,) \ , \tag{2.22}$$

where $\vec{\alpha}$ is defined in eq.(2.10). (If we define $\vec{\beta} = \vec{\eta}/D_s$ and $\vec{\theta} = \vec{\xi}/D_d$ we get eq.(2.13)). One can also write eq.(2.22) as follows

$$\nabla_{\vec{\xi}} \ \hat{\Phi}(\vec{\xi}, \vec{\eta}) = 0 \ , \tag{2.23}$$

which is an equivalent formulation of the Fermat principle.

The arrival time delay of light rays coming from two different images (due to the same source in $\vec{\eta}$) located in $\vec{\xi}^{\,(1)}$ and $\vec{\xi}^{\,(2)}$ is given by

$$c(t_1 - t_2) = \hat{\Phi}(\vec{\xi}^{\,(1)}, \vec{\eta}) - \hat{\Phi}(\vec{\xi}^{\,(2)}, \vec{\eta}) \ . \tag{2.24}$$

2.4 Remarks on the lens equation

It is often convenient to write (2.22) in a dimensionless form. Let ξ_0 be a length parameter in the lens plane (whose choice will depend on the specific problem) and let $\eta_0 = (D_s/D_d)\xi_0$ be the corresponding length in the source plane. We set $\vec{x} = \vec{\xi}/\xi_0, \quad \vec{y} = \vec{\eta}/\eta_0$ and

$$\kappa(\vec{x}) = \frac{\Sigma(\xi_0\vec{x})}{\Sigma_{crit}} \ , \qquad \vec{\alpha}(\vec{x}) = \frac{D_d D_{ds}}{\xi_0 D_s}\hat{\vec{\alpha}}(\xi_0\vec{x}) \ , \tag{2.25}$$

where we have defined a critical surface mass density

$$\Sigma_{crit} = \frac{c^2}{4\pi G}\frac{D_s}{D_d D_{ds}} = 0.35\ g\ cm^{-2}\left(\frac{1\ Gpc}{D}\right) \tag{2.26}$$

with $D \equiv \frac{D_d D_{ds}}{D_s}$ ($1\ Gpc = 10^9\ pc$). Then eq. (2.22) reads as follows

$$\vec{y} = \vec{x} - \vec{\alpha}(\vec{x})\ , \tag{2.27}$$

with

$$\vec{\alpha}(\vec{x}) = \frac{1}{\pi}\int_{R^2}\frac{\vec{x}-\vec{x}'}{\mid \vec{x}-\vec{x}' \mid^2}\kappa(\vec{x}')d^2x'\ . \tag{2.28}$$

In the following we will mainly use the previous notation rather than the above one.

An interesting case is a lens with a constant surface mass density Σ. With eq.(2.11) one finds then for the deflection angle

$$\alpha(\theta) = \frac{4G}{c^2\xi}\ \Sigma\pi\xi^2 = \frac{4\pi G\Sigma}{c^2}\ D_d\theta\ , \tag{2.29}$$

using $\xi = D_d\theta$. In this case the lens equation (2.13) is linear, which means that β is proportional to θ

$$\beta = \theta - \beta = \theta - \frac{4\pi G}{c^2}\frac{D_{ds}D_d}{D_s}\ \Sigma\ \theta = \theta - \frac{\Sigma}{\Sigma_{crit}}\theta\ . \tag{2.30}$$

From eq.(2.30) we immediately see that for a lens with a critical surface mass density we get for all values of θ: $\beta = 0$. Such a lens would perfectly focus, with a well defined focal length. Typical gravitational lenses behave, however, quite differently. A lens which has $\Sigma > \Sigma_{crit}$ somewhere in it is defined as *supercritical*, and has in general multiple images.

Defining $k(\vec{\theta}\ ) := \Sigma(\vec{\theta}D_d)/\Sigma_{crit}$ we can write the lens equation as follows

$$\vec{\beta} = \vec{\theta} - \vec{\tilde{\alpha}}(\vec{\theta}\ )\ , \tag{2.31}$$

with

$$\vec{\tilde{\alpha}}(\vec{\theta}\ ) = \frac{1}{\pi}\int_{R^2} d^2\theta'\ k(\vec{\theta}')\ \frac{\vec{\theta}-\vec{\theta}'}{\mid \vec{\theta}-\vec{\theta}' \mid^2}\ . \tag{2.32}$$

Moreover

$$\vec{\tilde{\alpha}}(\vec{\theta}\ ) = \nabla_{\vec{\theta}}\ \Psi(\vec{\theta}\ ) \tag{2.33}$$

where

$$\Psi(\vec{\theta}\ ) = \frac{1}{\pi}\int_{R^2} d^2\theta' k(\vec{\theta}')\ ln\mid \vec{\theta}-\vec{\theta}' \mid\ . \tag{2.34}$$

The Fermat potential is given by

$$\Phi(\vec{\theta},\vec{\beta}\,) = \frac{1}{2}(\vec{\theta}-\vec{\beta}\,)^2 - \Psi(\vec{\theta}\,) \tag{2.35}$$

and we get then the lens equation from

$$\nabla_{\vec{\theta}}\,\Phi(\vec{\theta},\vec{\beta}) = 0\ . \tag{2.36}$$

Notice that

$$\Delta\Psi = 2k \geq 0 \tag{2.37}$$

(using $\Delta\ ln\mid\vec{\theta}\mid = 2\pi\delta^2(\vec{\theta}\,)$), since k as a surface mass density is always positive (or vanishes).

The flux of a source, located in $\vec{\beta}$, in the solid angle $d\Omega(\vec{\beta}\,)$ is given by

$$S(\vec{\beta}\,) = I_\nu\ d\Omega(\vec{\beta}\,)\ . \tag{2.38}$$

I_ν is the intensity of the source in the frequency ν. $S(\vec{\beta}\,)$ is the flux one would see if there were no lensing. On the other hand the observed flux from the image located in $\vec{\theta}$ is

$$S(\vec{\theta}\,) = I_\nu\ d\Omega(\vec{\theta}\,)\ . \tag{2.39}$$

I_ν does not change, since the total number of photons stays constant as well as their frequency. The amplification factor μ is thus given by the ratio

$$\mu = \frac{d\Omega(\vec{\theta}\,)}{d\Omega(\vec{\beta}\,)} = \frac{1}{detA(\vec{\theta}\,)}\ , \tag{2.40}$$

with

$$A(\vec{\theta}\,) = \frac{d\vec{\beta}}{d\vec{\theta}}\ \ (A_{ij} = \frac{d\beta_i}{d\theta_j} = \delta_{ij} - \Psi_{,ij})\ , \tag{2.41}$$

(where $\Psi_{,ij} = \partial_i\partial_j\Psi$) which is the Jacobi matrix of the corresponding lens mapping given by eq.(2.31). Notice that the amplification factor μ can be positive or negative. The corresponding image will then have *positive or negative parity*, respectively.

For some values of $\vec{\theta}$, $detA(\vec{\theta}\,) = 0$ and thus $\mu \to \infty$. The points (or the curve) $\vec{\theta}$ in the lens plane for which $detA(\vec{\theta}\,) = 0$ are defined as *critical points (or critical curve)* . At these points the geometrical optics approximation used so far breaks down. The corresponding points (or curve) of the critical points in the source plane are the so called *caustics* .

The matrix A_{ij} is often parametrized as follows

$$A_{ij} = \begin{pmatrix} 1-k-\gamma_1 & -\gamma_2 \\ -\gamma_2 & 1-k+\gamma_1 \end{pmatrix} \tag{2.42}$$

with $\gamma_1 = \frac{1}{2}(\Psi_{,11} - \Psi_{,22})$, $\gamma_2 = \Psi_{,12} = \Psi_{,21}$ and $\vec{\gamma} = (\gamma_1, \gamma_2)$. We have therefore

$$detA_{ij} = (1-k)^2 - \gamma^2 \tag{2.43}$$

and $\gamma = \sqrt{\gamma_1^2 + \gamma_2^2}$,

$$trA_{ij} = 2(1-k) \ . \tag{2.44}$$

The eigenvalues of A_{ij} are $a_{1,2} = 1 - k \pm \gamma$.

As next, we study how small circles in the source plane are deformed. Consider a small circular source with radius R at $\vec{y}$, bounded by a curve described by

$$\vec{c}(t) = \vec{y} + \begin{pmatrix} R\ \cos t \\ R\ \sin t \end{pmatrix} \qquad (0 \leq t \leq 2\pi) \ . \tag{2.45}$$

The corresponding boundary curve of the image is

$$\vec{d}(t) = \vec{x} + A^{-1} \begin{pmatrix} R\ \cos t \\ R\ \sin t \end{pmatrix} . \tag{2.46}$$

Inserting the parametrization (2.42) one finds that the image is an ellipse centered on $\vec{x}$ with semi–axes parallel to the main axes of A, with magnitudes

$$\frac{R}{\mid 1 - \kappa \pm \gamma \mid} \ , \tag{2.47}$$

and the position angles $\varphi_\pm$ for the axes are

$$\tan\varphi_\pm = \frac{\gamma_1}{\gamma_2} \mp \sqrt{\left(\frac{\gamma_1}{\gamma_2}\right)^2 + 1} \ or \qquad \tan 2\varphi_\pm = -\frac{\gamma_2}{\gamma_1} \ . \tag{2.48}$$

The ellipticity of the image is defined as follows

$$\epsilon = \epsilon_1 + i\epsilon_2 = \frac{1-r}{1+r} e^{2i\varphi} \ , \quad r \equiv \frac{b}{a} \ , \tag{2.49}$$

where φ is the position angle of the ellipse and a and b are the major and minor semiaxes, respectively. a and b are proportional to the inverse of the eigenvalues of the matrix A_{ij} defined in eq. (2.42), thus: $a = R(1-k-\gamma)^{-1}$ and $b = R(1-k+\gamma)^{-1}$. ϵ describes the orientation and the shape of the ellipse and is thus observable. Lets denote $g = \mid \epsilon \mid$ with

$$g = \frac{\gamma}{1-\kappa} \qquad \left(\vec{g} = \frac{\vec{\gamma}}{1-\kappa}\right) \ , \tag{2.50}$$

which is called the *reduced shear*. Often one uses a complex notation with $\gamma = \gamma_1 + i\gamma_2$ and accordingly one defines then a complex reduced shear.

2.4.1 Classification ordinary images

If we consider a fixed value for $\vec{\beta}$, then $\Phi(\vec{\theta},\vec{\beta})$ defines a (two-dimensional) surface for the arrival time of the light. Ordinary images, for which $detA(\vec{\theta}\,) \neq 0$, are formed at the points $\vec{\theta}$, where $\nabla_{\vec{\theta}}\,\Phi(\vec{\theta},\vec{\beta}) = 0$. Thus the images are localized at extremal or saddle points of the surface $\Phi(\vec{\theta},\vec{\beta})$ and are classified as follows.

Images of type I:
correspond to minima of Φ, with $detA > 0$, $trA > 0$ (and thus: $\gamma < 1-k \leq 1$, $a_i > 0$, $\mu \geq \frac{1}{1-\gamma^2} \geq 1$).

Images of type II:
correspond to saddle points of Φ, with $detA < 0$ (then: $(1-k)^2 < \gamma^2$, $a_2 > 0 > a_1$).

Images of type III:
correspond to maxima of Φ, with $detA > 0$, $trA < 0$ (with $(1-k)^2 > \gamma^2$, $k > 1$, $a_i < 0$).

Consider a thin lens with a smooth surface mass density $k(\vec{\theta}\,)$, which decreases faster than $\mid \vec{\theta}\mid^{-2}$ for $\mid \vec{\theta}\mid \rightarrow \infty$. For such a lens the total mass is finite and the deflection angle $\vec{\alpha}(\vec{\theta}\,)$ is continuous and tends to zero for $\mid \vec{\theta}\mid \rightarrow \infty$, therefore $\vec{\alpha}$ is bounded: $\mid \vec{\alpha}\mid \leq \alpha_0$. Moreover, lets denote by n_I the number of images of type I for a source located in $\vec{\beta}$, similarly for n_{II} and n_{III} and define $n_{tot} = n_I + n_{II} + n_{III}$. If these conditions are fulfilled than the following theorems hold.

Theorem 1

If the above conditions hold and $\vec{\beta}$ is not situated on a caustic, the following conditions apply:

a) $n_I \geq 1$
b) $n_{tot} < \infty$
c) $n_I + n_{III} = 1 + n_{II}$
d) for $\mid \vec{\beta}\mid$ sufficiently large $n_{tot} = n_I = 1$.

It thus follows from c) that the total number of images $n_{tot} = 1 + 2n_{II}$ is odd. The number of images with positive parity $(n_I + n_{III})$ exceeds by one those with negative parity (n_{II}); $n_{II} \geq n_{III}$ and $n_{tot} > 1$ if and only if $n_{II} \geq 1$. The number of images is odd, however, in practice some images may be very faint or be covered by the lens itself and are thus not

observable.

Theorem 2

The image of the source which will appear first to the observer is of type I and it is at least as bright as the unlensed source would appear ($\mu(\vec{\theta}_1) \geq 1$).

For a proof of the two theorems we refer to [4]. The second theorem is a consequence of the fact that the surface mass density k is a positive quantity.

Chapter 3

Simple lens models

3.1 Axially symmetric lenses

Lets consider a lens with an axially symmetric surface mass density, that is $\Sigma(\vec{\xi}) = \Sigma(\mid \vec{\xi} \mid)$, in which case the lens equation reduces to a one-dimensional equation. By symmetry we can restrict the impact vector $\vec{\theta}$ to be on the positive θ_1-axis, thus we have $\vec{\theta} = (\theta, 0)$ with $\theta > 0$. We can then use polar coordinates: $\vec{\theta'} = \theta'(cos\phi, sin\phi)$ (thus $d^2\theta' = \theta' d\theta' d\phi$). With $k(\vec{\theta}) = k(\theta)$ we get for eq.(2.32)

$$\alpha_1(\theta) = \frac{1}{\pi} \int_0^\infty \theta' \; d\theta' k(\theta') \; \int_0^{2\pi} d\phi \; \frac{\theta - \theta' cos\phi}{\theta^2 + \theta'^2 - 2\theta\theta' cos\phi} \; , \tag{3.1}$$

$$\alpha_2(\theta) = \frac{1}{\pi} \int_0^\infty \theta' \; d\theta' k(\theta') \; \int_0^{2\pi} d\phi \; \frac{-\theta' sin\phi}{\theta^2 + \theta'^2 - 2\theta\theta' cos\phi} \; . \tag{3.2}$$

Due to the symmetry $\vec{\alpha}$ is parallel to $\vec{\theta}$ and with eq. (3.2) we get $\alpha_2(\theta) = 0$. Only the mass inside the disc of radius θ around the center of the lens contributes to the light deflection, therefore from eq. (3.1) one finds

$$\alpha(\theta) \equiv \alpha_1(\theta) = \frac{2}{\theta} \int_0^\theta \theta' \; d\theta' k(\theta') \equiv \frac{m(\theta)}{\theta} \; . \tag{3.3}$$

This way we can write the lens equation as

$$\beta = \theta - \alpha(\theta) = \theta - \frac{m(\theta)}{\theta} \tag{3.4}$$

for $\theta \geq 0$. Due to the axial symmetry it is enough to consider $\beta \geq 0$. Since $m(\theta) \geq 0$ it follows that $\theta \geq \beta$ (for $\theta \geq 0$). Instead of eq. (2.34) we get

$$\Psi(\theta) = 2 \int_0^\theta \theta' \; d\theta' \; k(\theta') \; ln \left(\frac{\theta}{\theta'} \right) \; , \tag{3.5}$$

whereas the Fermat potential can be written as

$$\Phi(\theta,\beta) = \frac{1}{2}(\theta-\beta)^2 - \Psi(\theta) \ . \tag{3.6}$$

This way we get the lens equation (3.4) from

$$\frac{\partial\Phi(\theta,\beta)}{\partial\theta} = 0 \ . \tag{3.7}$$

To get the Jacobi matrix we write: $\vec{\alpha}(\vec{\theta}) = \frac{m(\theta)}{\theta^2}\vec{\theta}$ (with $\vec{\theta} = (\theta_1,\theta_2)$ and $\theta = \mid \vec{\theta} \mid$) and thus

$$A = \begin{pmatrix} 1 & 0 \\ 0 & 1 \end{pmatrix} - \frac{m(\theta)}{\theta^4}\begin{pmatrix} \theta_2^2-\theta_1^2 & -2\theta_1\theta_2 \\ -2\theta_1\theta_2 & \theta_1^2-\theta_2^2 \end{pmatrix} - \frac{2k(\theta)}{\theta^2}\begin{pmatrix} \theta_1^2 & \theta_1\theta_2 \\ \theta_1\theta_2 & \theta_2^2 \end{pmatrix} , \tag{3.8}$$

where we made use of $m'(\theta) = 2\theta k(\theta)$. The determinant of the Jacobi matrix is given by

$$detA = \left(1-\frac{m}{\theta^2}\right)\left(1-\frac{d}{d\theta}\left(\frac{m}{\theta}\right)\right) = \left(1-\frac{m}{\theta^2}\right)\left(1+\frac{m}{\theta^2}-2k\right) \ . \tag{3.9}$$

3.1.1 Tangential and radial critical curves

The critical curves (the points for which $detA(\theta) = 0$) are then circles of radius θ. From eq.(3.9) we see that there are two possible cases:

(i) $\frac{m}{\theta^2} = 1$: defined as *tangential critical curve*;

(ii) $\frac{d}{d\theta}\left(\frac{m}{\theta}\right) = 1$: defined as *radial critical curve*.

For case (i) one gets $\frac{m}{\theta} = \theta$ and thus from the lens equation (3.4) we see that $\beta = 0$ is the corresponding caustic, which reduces to a point. If the axial symmetric gets only slightly perturbed this degeneracy is lifted.

We can look at the critical points on the θ_1-axis with $\vec{\theta} = (\theta,0), \theta > 0$. Then

$$A = 1 - \frac{m(\theta)}{\theta^2}\begin{pmatrix} -1 & 0 \\ 0 & +1 \end{pmatrix} - \frac{m'}{\theta}\begin{pmatrix} 1 & 0 \\ 0 & 0 \end{pmatrix} \tag{3.10}$$

and this matrix must have an eigenvector $\vec{X}$ with eigenvalue zero. For symmetry reasons, the vector must be either tangential, $\vec{X} = (0,1)$, or normal, $\vec{X} = (1,0)$, to the critical curve (which must be a circle). We see readily that the first case occurs for a tangential critical curve, and the second for a radial critical curve. The image of a circle (in the source plane) which lies close to a tangential critical curve will be deformed to an ellipse with major axis tangential to the critical curve. On the other hand if the

image of a circle gets close to a radial critical curve it will be deformed to an ellipse with major axis radial to the critical curve.

For a tangential critical curve ($|\vec{\theta}| = \theta_t$) we get

$$m(\theta_t) = \int_0^{\theta_t} 2\theta\kappa(\theta)d\theta = \theta_t^2. \tag{3.11}$$

With the definition of κ this translates to

$$\int_0^{\xi_t} 2\xi\Sigma(\xi)d\xi = \xi_t^2\Sigma_{crit}. \tag{3.12}$$

The total mass $M(\xi_t)$ inside the critical curve is thus

$$M(\xi_t) = \pi\xi_t^2\Sigma_{crit}. \tag{3.13}$$

This shows that the average density $\langle\Sigma\rangle_t$ inside the tangential critical curve is equal to the critical density Σ_{crit}. This can be used to estimate the mass of a deflector if the lens is sufficiently strong and the geometry is such that almost complete Einstein rings are formed (see Chapter 6).

3.1.2 Einstein radius

For a lens with axial symmetry we get, with (2.11), the following equation

$$\beta(\theta) = \theta - \frac{D_{ds}}{D_s D_d}\frac{4GM(\theta)}{c^2\theta}\ , \tag{3.14}$$

from which we see that the image of a source, which is perfectly aligned (that means $\beta = 0$), is a ring if the lens is supercritical. By setting $\beta = 0$ in eq.(3.14) we get the radius of the ring

$$\theta_E = \left(\frac{4GM(\theta_E)}{c^2}\frac{D_{ds}}{D_d D_s}\right)^{1/2}\ , \tag{3.15}$$

which is called *Einstein radius*. The Einstein radius depends not only on the characteristics of the lens but also on the various distances.

The Einstein radius sets a natural scale for the angles entering the description of the lens. Indeed, for multiple images the typical angular separation between the different images turns out to be of order $2\theta_E$. Moreover, sources with angular distance smaller than θ_E from the optical axis of the system get magnified quite substantially whereas sources which are at a distance much greater than θ_E are only weakly magnified.

In several lens model the Einstein radius delimits the region within which multiple images occur, whereas outside there is a single image. By comparing eq.(2.26) with eq.(3.15) we see that the surface mass density

inside the Einstein radius precisely corresponds to the critical density. For a point-like lens with mass M the Einstein radius is given by

$$\theta_E = \left(\frac{4GM}{c^2} \frac{D_{ds}}{D_d D_s} \right)^{1/2} , \tag{3.16}$$

or instead of an angle one often uses also

$$R_E = \theta_E D_d = \left(\frac{4GM}{c^2} \frac{D_{ds} D_d}{D_s} \right)^{1/2} . \tag{3.17}$$

To get some typical values we can consider the following two cases: a lens of mass M located in the galactic halo at a distance of $D_d \sim 10$ kpc and a source in the Magellanic Cloud, in which case

$$\theta_E = (0.9'' \times 10^{-3}) \left(\frac{M}{M_\odot} \right)^{1/2} \left(\frac{D}{10\ kpc} \right)^{-1/2} \tag{3.18}$$

and a lens with the mass of galaxy (including its halo) $M \sim 10^{12} M_\odot$ located at a distance of $D_d \sim 1$ Gpc

$$\theta_E = 0.9'' \left(\frac{M}{10^{12} M_\odot} \right)^{1/2} \left(\frac{D}{Gpc} \right)^{-1/2} , \tag{3.19}$$

where $D = D_d D_s / D_{ds}$.

3.2 Schwarzschild lens

A particular case of a lens with axial symmetry is the Schwarzschild lens, for which $\Sigma(\vec{\xi}) = M\delta^2(\vec{\xi})$ and thus $m(\theta) = \theta_E^2$. The source is also considered as point-like, this way we get for the lens equation (2.13) the following expression

$$\beta = \theta - \frac{\theta_E^2}{\theta} , \tag{3.20}$$

where θ_E is given by eq. (3.16). This equation has two solutions

$$\theta_\pm = \frac{1}{2} (\beta \pm \sqrt{\beta^2 + 4\theta_E^2}) . \tag{3.21}$$

Therefore, there will be two images of the source located one inside the Einstein radius and the other outside. For a lens with axial symmetry the amplification is given by

$$\mu = \frac{\theta}{\beta} \frac{d\theta}{d\beta} . \tag{3.22}$$

For the Schwarzschild lens, which is a limiting case of an axial symmetric one, we can substitute β using eq.(3.21) and obtain this way the amplification for the two images

$$\mu_{\pm} = \left[1 - \left(\frac{\theta_E}{\theta_{\pm}}\right)^4\right]^{-1} = \frac{u^2+2}{2u\sqrt{u^2+4}} \pm \frac{1}{2} \; . \tag{3.23}$$

$u = r/R_E$ is the ratio between the impact parameter r, that is the distance between the lens and the line of sight connecting the observer and the source and the Einstein radius R_E defined in eq.(3.17). u can also be expressed as β/θ_E. Since $\theta_- < \theta_E$ we have that $\mu_- < 0$. The negative sign for the amplification indicates that the parity of the image is inverted with respect to the source. The total amplification is given by the sum of the absolute values of the amplifications for each image

$$\mu = \mid \mu_+ \mid + \mid \mu_- \mid = \frac{u^2+2}{u\sqrt{u^2+4}} \; . \tag{3.24}$$

If $r = R_E$ then we get $u = 1$ and $\mu = 1.34$, which corresponds to an increase of the apparent magnitude of the source of $\Delta m = -2.5 \; log\mu = -0.32$. For lenses with a mass of the order of a solar mass and which are located in the halo of our galaxy the angular separation between the two images is far too small to be observable. Instead, one observes a time dependent change in the brightness of the the source star. This situation is also referred to as *microlensing*.

Much research activity is devoted to study microlensing in the context of quasar lensing. Today, several cases of quasars are known which are lensed by foreground galaxies, producing multiple observable images. The stars contained in the lensing galaxy can act as microlenses on the quasar and as a result induce time-dependent changes in the quasar brightness, but in a rather complicated way, since here the magnification is a coherent effect of many stars at the same time. This is an interesting field of research, which will lead to important results on the problem of the dark matter in galaxies [15]. However, we will not discuss *extragalactic* microlensing in detail (see for instance [16]), whereas we will report in some depth on *galactic* microlensing (see Chapter 4).

The time delay between the two images of a Schwarzschild lens is given by

$$c\Delta t = \frac{4GM}{c^2}\left(\frac{1}{2}u\sqrt{u^2+4} + ln\frac{\sqrt{u^2+4}+u}{\sqrt{u^2+4}-u}\right) \; . \tag{3.25}$$

The two images have a comparable luminosity only if $u \leq 1$ (otherwise the difference is such that one image is no longer observable since it gets too faint). For $u = 1$ one gets $\Delta t \sim \frac{4R_S}{c}$ (typically for a galaxy with mass

$M = 10^{12}\, M_\odot$ one finds $\Delta t \sim 1.3$ years). Such measurements are important since they allow to determine the value H_0 of the Hubble constant (see Section 5.1).

3.3 Singular isothermal sphere

A simple model for describing the matter distribution in a galaxy is to assume that the stars forming the galaxy behave like the particles in an ideal gas, confined by the total gravitational potential, which we assume to have spherical shape. The equation of state of the "particles" (stars) has the form

$$p = \frac{\rho k_B T}{m} \ , \tag{3.26}$$

where ρ and m are the matter density and the mass of a star, respectively. In the equilibrium case the temperature T is defined via the one-dimensional dispersion velocity σ_v of the stars as obtained from

$$m\sigma_v^2 = k_B T \ . \tag{3.27}$$

In principle the temperature could depend on the radius, however in the simplest model, of the isothermal spherical model, one assumes that the temperature is constant and so also σ_v. The equation for hydrostatic equilibrium is given by

$$\frac{p'}{\rho} = -\frac{GM(r)}{r^2} \ , \tag{3.28}$$

with

$$M'(r) = 4\pi r^2 \rho \ , \tag{3.29}$$

where $M(r)$ is the mass inside the sphere of radius r. A solution of the previous equations is

$$\rho(r) = \frac{\sigma_v^2}{2\pi G}\frac{1}{r^2} \ . \tag{3.30}$$

This mass distribution is called *singular isothermal sphere* (it is indeed singular for $r \to 0$). Since $\rho(r) \sim r^2$, $M(r) \sim r$, the velocity of the stars in the gravitational field of an isothermal sphere is given by

$$v_{rot}^2(r) = \frac{GM(r)}{r} = 2\sigma_v^2 \ , \tag{3.31}$$

which is constant. Such a mass distribution can (at least in a qualitative way) describe the flat rotation curves of the galaxies, as measured beyond a certain galactic radius. Thus the dark matter in the halo can in a first approximation be described by a singular isothermal sphere model.

The projected mass density on the lens plane perpendicular to the line of sight is as follows

$$\Sigma(\xi) = \frac{\sigma_v^2}{2G}\frac{1}{\xi} \ , \tag{3.32}$$

where ξ is the distance (in the lens plane) from the the center of mass. For the light deflction angle we get

$$\hat{\alpha} = 4\pi\frac{\sigma_v^2}{c^2} = 1.4'' \left(\frac{\sigma_v}{220\ km\ s^{-1}}\right)^2 \tag{3.33}$$

independent of the position ξ ($220\ km\ s^{-1}$ is a typical value for the rotation velocity in spiral galaxies).

The Einstein radius R_E is given by

$$R_E = 4\pi\frac{\sigma_v^2}{c^2}\frac{D_{ds}D_d}{D_s} = \hat{\alpha}\frac{D_{ds}D_d}{D_s} = \alpha D_d \ . \tag{3.34}$$

Multiple images occur only if the source is located within the Einstein radius. Let be $\xi_0 = R_E$, then $\Sigma(\xi) = \Sigma(x\xi_0)$ where $x = \xi/\xi_0$. This way the lens equation becomes

$$y = x - \frac{x}{\mid x \mid} \ . \tag{3.35}$$

For $0 < y < 1$ we have two solutions: $x = y + 1$ and $x = y - 1$. For $y > 1$ (the source is located outside the Einstein radius) there is only one image: $x = y + 1$. The images with $x > 0$ are of type I, whereas the ones with $x < 0$ are of type II. If the singularity in $\xi = 0$ is removed then there will be a third image in the center.

The amplification of an image in x is given by

$$\mu = \frac{\mid x \mid}{\mid x \mid -1} \tag{3.36}$$

(the circle $\mid x \mid = 1$ corresponds to a tangential critical curve). For $y \to 1$ the second image (corresponding to the solution $x = y - 1$) gets very faint.

The potential is given by $\psi(x) = \mid x \mid$ and the time delay between the images is

$$c\Delta t = \left(4\pi\left(\frac{\sigma_v}{c}\right)^2\right)^2 \frac{D_d D_{ds}}{D_s} 2y \ . \tag{3.37}$$

3.4 Generalization of the singular isothermal sphere

The singular isothermal sphere model can for instance be generalized by adopting for the projected mass density Σ the following expression

$$\Sigma(\xi) = \Sigma_0 \frac{1 + p(\xi/\xi_c)^2}{(1 + (\xi/\xi_c)^2)^{2-p}} \ , \tag{3.38}$$

with $0 \leq p \leq 1/2$ and Σ_0 is the central density. ξ_c is a typical distance of the order of the scale on which the matter decreases, often one can take it as the core radius of a galaxy. $p = 0$ corresponds to the Plummer distribution, whereas for $p = 1/2$ we get the isothermal sphere for large values of ξ.

Defining $x = \xi/\xi_0$ and $k_0 = \Sigma_0/\Sigma_{crit}$ we can write eq.(3.38) as

$$k(x) = k_0 \frac{1 + px^2}{(1 + x^2)^{2-p}} \ . \tag{3.39}$$

The deflection potential is given by

$$\Psi(x) = \frac{k_0}{2p} \ \left[(1 + x^2)^p - 1\right] \ , \tag{3.40}$$

which is valid for $p \neq 0$, whereas for $p = 0$ we get

$$\Psi(x) = \frac{k_0}{2} \ ln(1 + x^2) \ . \tag{3.41}$$

Thus the lens equation is

$$y = x - \alpha(x) = x - \frac{k_0 x}{(1 + x^2)^{1-p}} \ . \tag{3.42}$$

If $k_0 > 1$ there is one tangential critical curve for $x = x_t$, where $x_t = \sqrt{k_0^{1/1-p} - 1}$, and a radial critical curve for $x = x_r$, which is defined by the equation

$$1 - k_0(1 + x_r^2)^{p-2} \left[1 + (2p - 1)x_r^2\right] = 0 \ . \tag{3.43}$$

The corresponding caustics are given by $y_t \equiv y(x_t) = 0$, whereas

$$y_r \equiv \mid y(x_r) \mid = \frac{2(1 - p)x_r^3}{1 - (1 - 2p)x_r^2} \ . \tag{3.44}$$

Sources with $\mid y \mid < y_r$ lead to the formation of three images, whereas for $\mid y \mid > y_r$ there is only one image. The three images are at: $x > x_t$ (image of type I), $-x_t < x < r_r$ (image of type II) and $-x_r < x < 0$ (image of type III).

3.5 Extended source

The magnification for an extended source with surface brightness profile $I(\vec{y})$ is given by

$$\mu_e = \frac{\int I(\vec{y})\mu_p(\vec{y})d^2y}{\int I(\vec{y})d^2y} \ , \tag{3.45}$$

where $\mu_p(\vec{y})$ is the magnification of a point source at position $\vec{y}$. As an example lets consider a disklike source with radius R centered in $\vec{y}$ with a

brightness profile $I(r/R)$, where r is the distance of a source point from the center of the source. Adopting polar coordinates centered on the circular source, we obtain

$$\mu_e(y) = \left[2\pi \int_0^\infty I(r/R) r dr\right]^{-1} \int_0^\infty I(r/R) r dr \times \int_0^{2\pi} d\phi \frac{\mu_p(y) y}{\sqrt{y^2 + r^2 + 2ry cos\phi}} \ . \tag{3.46}$$

For a uniform brightness profile the maximum of μ_e is at $y = 0$ (with $\mu_e(0) = 2/R$ if μ_p is the magnification of a point source, since then $\mu_p(y)y \to 0$ for $y \to 0$). Indeed, for a Schwarzschild lens with $\mu_p = (y^2+2)/(y\sqrt{y^2+4})$ one finds

$$\mu_e^{max} = \frac{\sqrt{4 + R^2}}{R} \ . \tag{3.47}$$

3.6 Two point-mass lens

A natural generalization of the Schwarzschild lens is to consider a lens with two point masses. This case is also of relevance for the applications, since many binary microlensing events have been observed. For several point masses M_i located at transversal positions $\vec{\xi}_i$ the general formula eq.(2.10) for the deflection angle gives

$$\vec{\alpha}(\vec{\xi}) = \sum_{i=1}^{N} \frac{4GM_i}{c^2} \frac{\vec{\xi} - \vec{\xi}_i}{\mid \vec{\xi} - \vec{\xi} \mid^2} \ . \tag{3.48}$$

Let $M = \sum_i^N M_i$ be the total mass and $M_i = \eta_i M$. For the typical length scale ξ_0 we chose the Einstein radius eq.(3.17) for the total mass. Then the lens map becomes

$$\vec{y} = \vec{x} - \sum_{1=1}^{N} \frac{\eta_i}{\mid \vec{x} - \vec{x}_i \mid^2} (\vec{x} - \vec{x}_i) \ , \tag{3.49}$$

where $\vec{x}_i = \vec{\xi}_i/\xi_0$. For a detailed discussion see [4].

Chapter 4

Galactic microlensing

4.1 Introduction

There are cases in which the deflection angles are tiny, of the order of milliarcseconds or smaller, such that the multiple images are not observable. However, lensing magnifies the affected source, and since the lens and the source are moving relative to each other, this can be detected as a time-variable brightness. This behaviour is referred to as gravitational microlensing, a powerful method to search for dark matter in the halo of our own Galaxy, if it consists of massive astrophysical compact halo objects (MACHOs), and to study the content of low-mass stars in the galactic disk.

The idea to use gravitational light deflection to detect MACHOs in the halo of our Galaxy by monitoring the light variability of millions of stars in the Large Magellanic Cloud (LMC) was first proposed by Paczyński in 1986 [17] and then further developed – from a theoretical point of view – in a series of papers by De Rújula, Jetzer and Massó [18, 19], Griest [20] and Nemiroff [21]. Following these first studies, the field has grown very rapidly, especially since the discovery of the first microlensing events at the end of 1993 and many new applications have been suggested, including the detection of Earth like planets around stars in our Galaxy. (For reviews on microlensing see for instance ref. [22, 23, 24, 25]).

Since the discovery of the first microlensing events in September 1993 by monitoring millions of stars in the Large Magellanic Cloud (LMC) and in the direction of the galactic centre, several hundreds of events have been found. The still few observed events towards the LMC indicate that the halo dark matter fraction in the form of MACHOs is of the order of 20%, assuming a standard spherical halo model.

The best evidence for dark matter in galaxies comes from the observed rotation curves in spiral galaxies. Measurements of the rotation velocity v_{rot} of stars up to the visible edge of the spiral galaxies (of about 10 kpc) and of atomic hydrogen gas in the disk beyond the optical radius (by mea-

suring the Doppler shift in the characteristic 21-cm radio line emitted by neutral hydrogen gas) imply that v_{rot} remains constant out to very large distances, rather than showing a Keplerian fall-off, as expected if there is no more matter beyond the visible edge.

There are also measurements of the rotation velocity for our own Galaxy. However, these observations turn out to be rather difficult, and the rotation curve has been measured accurately only up to a distance of about 20 kpc. Without any doubt, our own Galaxy has a typical flat rotation curve and thus it is possible to search directly for dark matter characteristic of spiral galaxies in the Milky Way.

The question which naturally arises is what is the nature of dark matter in galactic halos? A possibility is that the dark matter is comprised of baryons, which have been processed into compact objects (MACHOs) , such as stellar remnants (for a detailed discussion see ref. [26]). If their mass is below $\sim 0.08\ M_{\odot}$, they are too light to ignite hydrogen-burning reactions. Otherwise, MACHOs might be either low-mass ($\sim 0.1-0.3\ M_{\odot}$) hydrogen burning stars (also called M-dwarfs) or white dwarfs. As a matter of fact, a deeper analysis makes the M-dwarf option look problematic. The null result of several searches for low-mass stars both in the disk and in the halo of our Galaxy suggests that the halo cannot be mostly in the form of hydrogen-burning main-sequence M-dwarfs. Optical imaging of high-latitude fields taken with the Wide Field Planetary Camera of the Hubble Space Telescope indicates that less than $\sim 6\%$ of the halo can be in this form [27]. However, this result is derived under the assumption of a smooth spatial distribution of M-dwarfs, and the problem becomes considerably less severe in the case of a clumpy distribution [28]. Recent observations of four nearby spiral galaxies carried out with the satellite Infrared Space Observatory (ISO) seem also to exclude M-dwarfs as significantly contributing to halo dark matter [29].

A scenario with white dwarfs as a major constituent of the galactic halo dark matter has been explored [30]. However, it requires a rather ad hoc initial mass function sharply peaked around 2 - 6 $M_{\odot}$. Future Hubble deep-field exposures could either find the white dwarfs or put constraints on their fraction in the halo [31]. A substantial component of neutron stars and black holes with masses higher than $\sim 1\ M_{\odot}$ is also excluded, for otherwise they would lead to an overproduction of heavy elements relative to the observed abundances.

A further possibility is that the hydrogen gas is in molecular form, clumped into very cold clouds, as we proposed some years ago [32, 33]. Indeed, the observation of such clouds is very difficult and, therefore, at present there are no stringent limits on their contribution to the halo dark matter [34].

4.1.1 Microlensing probability

When a MACHO of mass M is sufficiently close to the line of sight between us and a more distant star, the light from the source star suffers a gravitational deflection and we see two images of the source (Fig. 4.1). For most applications we can consider the lens and the source as pointlike and thus use the Schwarzschild lens approximation as discussed in Section 3.2. R_E is then defined in eq.(3.17).

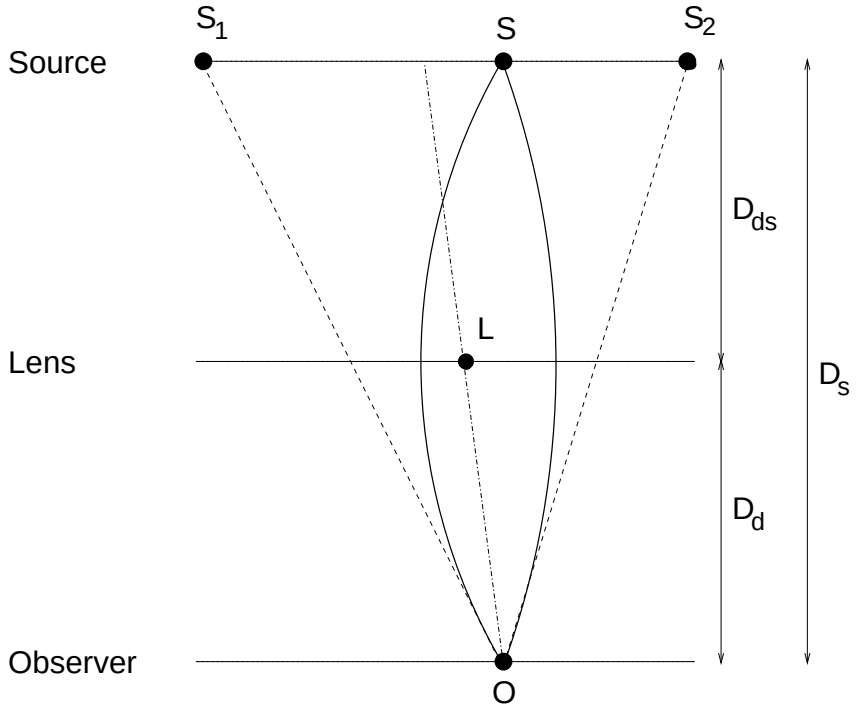

Figure 4.1. Setup of a gravitational lens situation: The lens L located between source S and observer O produces two images S_1 and S_2 of the background source. D_d is the distance between the observer and the lens, D_s between the observer and the source and D_{ds} between the lens and the source.

For a cosmological situation, where the lens is a galaxy or even a cluster of galaxies and the source is a very distant quasar, one indeed sees two or more images which are typically separated by an angle of some arcseconds. However, in the situation being considered here, namely of a MACHO of typically $\sim 0.1\ M_\odot$ and a source star located in the LMC at about 50 kpc from us, the separation angle turns out to be of the order of some milliarcseconds. Thus, the images cannot be seen separately. However, the

measured brightness of the source star varies with time. It increases until the MACHO gets to the shortest distance from the line of sight between the observer on Earth and the source star. Afterwards, the brightness decreases and eventually returns to its usual unlensed value. The magnification of the original star brightness turns out to be typically of the order of 30% or even more, corresponding to an increase of at least 0.3 magnitudes of the source star (see Figs. 4.2, 4.3). Such an increase is easily observable.

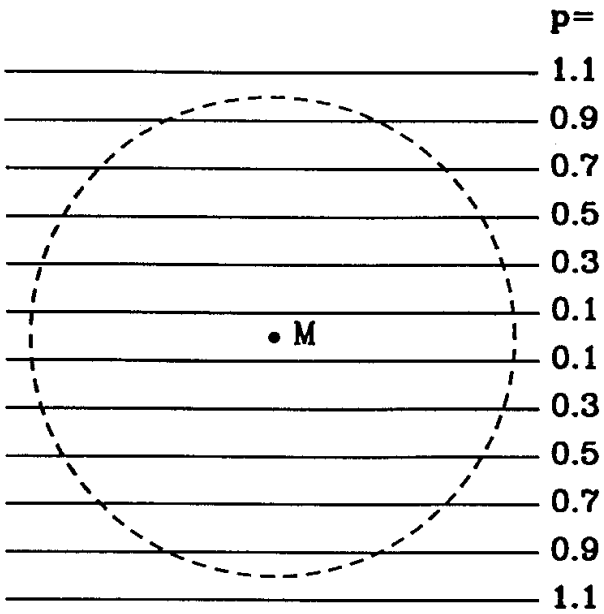

Figure 4.2. Einstein ring (dashed) and some possible relative orbits of a background star with projected minimal distances $p = r/R_E = 0.1, 0.3, ..., 1.1$ from a MACHO M (from [22]).

An important quantity is the optical depth τ due to gravitational microlensing, which is the probability that a source is found within a circle of radius $r \leq R_E$ around a MACHO. It is defined as follows

$$\tau = \int_0^1 dx \frac{4\pi G}{c^2} \rho(x) D_s^2 x(1-x) \tag{4.1}$$

with $\rho(x)$ being the mass density along the line of sight at distance $s = xD_s$ from the observer.

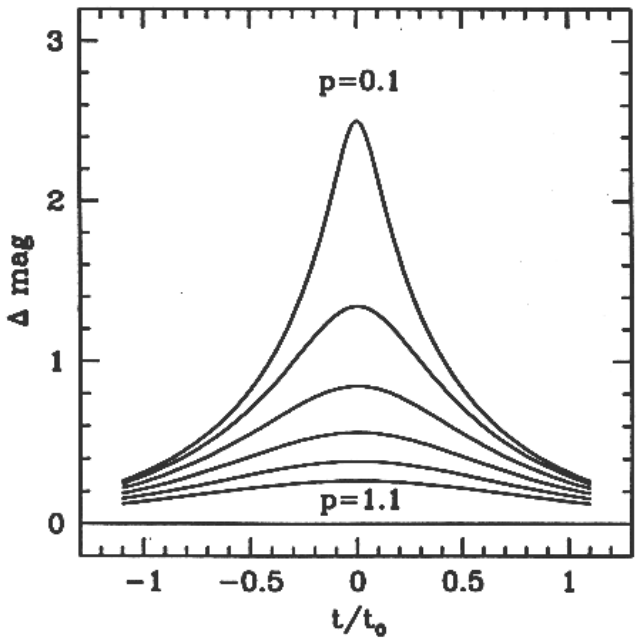

Figure 4.3. Light curves for the different cases of Fig. 4.2. The maximal magnification is $\Delta m = 0.32$ mag, if the star just touches the Einstein radius ($p = 1.0$). For smaller values of p the maximum magnification gets larger. t is the time in units of t_0 (from [22]).

We can easily compute τ assuming that the mass distribution in the galactic halo is of the following form

$$\rho(\vec{r}) = \frac{\rho_0(a^2 + R_{GC}^2)}{a^2 + \vec{r}^2} \ , \tag{4.2}$$

which is consistent with a flat rotation curve. $\mid \vec{r} \mid$ is the distance from Earth. a is the core radius, ρ_0 the local density nearby the solar system of dark matter and R_{GC} the distance to the galactic center. Standard values for these parameters are: $\rho_0 = 0.3\ GeV/cm^3 = 7.9 \times 10^{-3} M_\odot/pc^3$, $a = 5.6\ kpc$ e $R_{GC} = 8.5\ kpc$.

Assuming a spherical halo made entirely of MACHOs , one finds an optical depth towards the LMC of $\tau = 5 \times 10^{-7}$. This means that at any one moment out of 2 million stars, one is being lensed. From this number it can be seen that in order to obtain a reasonable number of microlensing

events, an experiment has to monitor several million stars in the LMC or in other targets such as the galactic centre region (referred also as the galactic bulge).

The magnification of the brightness of a star by a MACHO is a time-dependent effect, since the MACHO, which acts as lens, changes its location relative to the line of sight to the source as it moves along its orbit around the galaxy. Typically, the velocity transverse to the line of sight for a MACHO in the galactic halo is $v_T \approx 200$ km/s, which can be inferred from the measured rotation curve of our Galaxy. Clearly, the duration of the microlensing phenomenon and thus of the brightness increase of the source star depends on the MACHO mass, its distance and transverse velocity (see Table 1).

Since the light deflection does not depend on the frequency of the light, the change in luminosity of the source star will be achromatic. For this reason, the observations are done in different wavelengths in order to check that. Moreover, the light curve will be symmetric with respect to the maximum value, since the transverse velocity of the MACHO is in excellent approximation constant during the period in which the lensing occurs. The probability that a given star is lensed twice is practically zero. Therefore, the achromaticity, symmetry and uniqueness of the signal are distinctive features that allow a microlensing event to be discriminated from background events such as variable stars (some of which are periodic, others show chromaticity and most often the light curve is not symmetric).

4.1.2 Microlensing towards the LMC

Another important quantity is the microlensing rate, which depends on the mass and velocity distributions of MACHOs. To determine this one has to model the Galaxy and its halo. For simplicity one usually assumes a spherically symmetric shape for the halo with matter density decreasing as $1/r^2$ with distance as in eq.(4.2), to obtain naturally a flat rotation curve. The velocity distribution is assumed to be Maxwellian. The least known quantity is the mass distribution of the MACHOs. For that, one makes the simplifying assumption that all MACHOs have the same mass. The number N_{ev} of microlensing events (such that the increase in magnitude is at least 30%) can then be computed. Table 1 shows some values for N_{ev} assuming monitoring of a million stars for 1 year in the LMC.

Table 1 The expected number of events N_{ev} is obtained for a halo made entirely of MACHOs of a given mass.

MACHO mass ($M_\odot$)	Mean R_E (km)	Mean microlensing duration	N_{ev}
10^{-1}	0.3×10^9	1 month	4.5
10^{-2}	10^8	9 days	15
10^{-4}	10^7	1 day	165
10^{-6}	10^6	2 h	1662

Microlensing allows the detection of MACHOs located in the galactic halo in the mass range $10^{-7} < M/M_\odot < 1$ [19], as well as MACHOs in the disk or bulge of our Galaxy [35, 36].

In September 1993, the French collaboration EROS (Expérience de Recherche d'Objets Sombres) [37] announced the discovery of two microlensing candidates, and the American–Australian collaboration MACHO (for the collaboration they use the same acronym as for the compact objects) of one candidate [38] by monitoring several millions of stars in the LMC (Fig. 4.4).

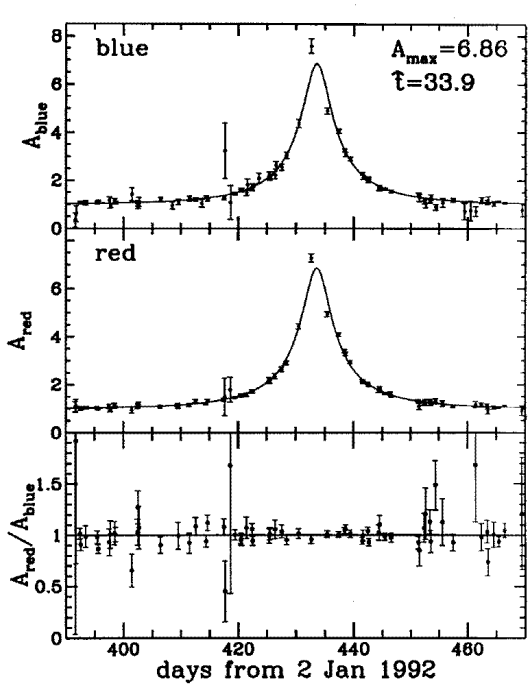

Figure 4.4. Microlensing event observed by the MACHO collaboration in their first year data towards the LMC. The event lasted about 33 days. The data are shown for blue light, red light and the ratio red light to blue light, which for perfect achromaticity should be equal to 1 (from [38]).

The MACHO team went on to report the observation of 13 to 17 events (one being a binary lensing event; see Fig. 4.5) by analysing their 5.7 years of LMC data [39]. The inferred optical depth is $\tau = 1.2^{+0.4}_{-0.3} \times 10^{-7}$ with an additional 20% to 30% of systematic error. Correspondingly, this implies that about 20% of the halo dark matter is in the form of MACHOs with a most likely mass in the range 0.15 - 0.9 $M_\odot$ depending on the halo model. Moreover, it might well be that not all the MACHOs are in the halo: some could be stars in the LMC itself or located in an extended disk of our Galaxy, in which case an average mass value including all events would produce an incorrect value. These considerations show that at present, the value for the average mass as well as the fraction of halo dark matter in form of MACHOs have to be treated with care.

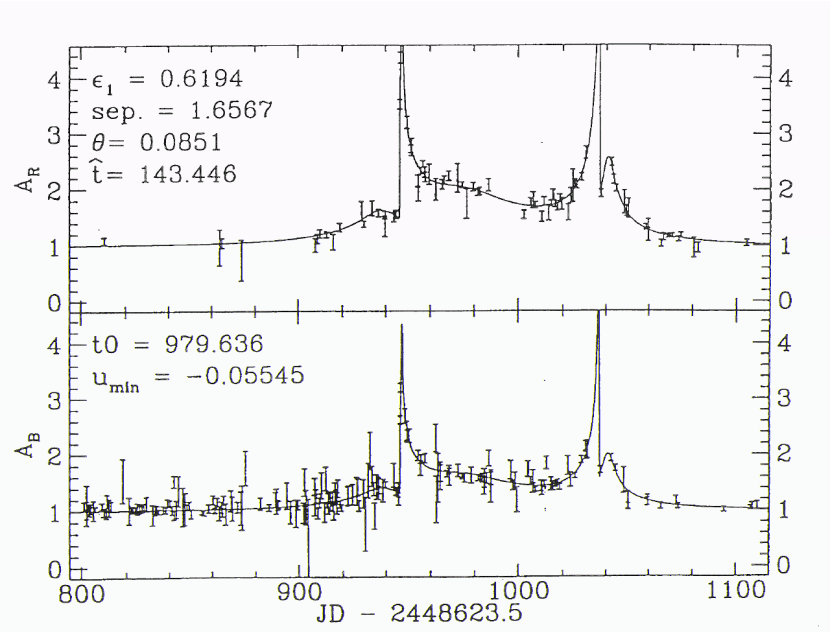

Figure 4.5. Binary microlensing event towards the LMC by the MACHO collaboration (taken from the web page http://darkstar.astro.washington.edu). The two light curves correspond to observations in different colors taken in order to test achromaticity.

As mentioned, one of the events discovered was due to a lens made of two objects, namely a binary system. Such events are more rare, but their observation is not surprising; since almost 50% of the stars are double systems, it is quite plausible that MACHOs also form binary systems. The

light curve is then more complicated than for a single MACHO.

EROS has also searched for very low mass MACHOs by looking for microlensing events with time scales ranging from 30 min to 7 days [40]. The lack of candidates in this range places significant constraints on any model for the halo that relies on objects in the range $5 \times 10^{-8} < M/M_{\odot} < 2 \times 10^{-2}$. Indeed, such objects may make up at most 20% of the halo dark matter (in the range between $5 \times 10^{-7} < M/M_{\odot} < 2 \times 10^{-3}$ at most 10%). Similar conclusions have also been reached by the MACHO group [39].

A few events have also been discovered towards the Small Magellanic Cloud [41, 42].

4.1.3 Microlensing towards other targets

To date, the MACHO [43] and OGLE collaborations have found several hundred microlensing events towards the galactic bulge, most of which are listed among the alert events, which are constantly updated [1]. During their first season, the MACHO team found 45 events towards the bulge, which led to an estimated optical depth of $\tau \simeq 2.43^{+0.54}_{-0.45} \times 10^{-6}$, which is roughly in agreement with the OGLE result [44], and also implies the presence of a bar in the galactic centre. They also found three events by monitoring the spiral arms of our Galaxy in the region of Gamma Scutum. Meanwhile, the EROS II collaboration also found some events towards the spiral arm regions. These results are important for studying the structure of our Galaxy [45].

Microlensing searches towards the Andromeda galaxy (M31) have also been proposed [46, 47, 48]. In this case, however, one has to use the so-called "pixel-lensing" method. Since the source stars are in general no longer resolvable, one has to consider the luminosity variation of a whole group of stars, which are, for instance, registered on a single pixel element of a CCD camera. This makes the subsequent analysis more difficult; on the other hand, if successful it allows M31 and other objects to be used as targets, which would otherwise not be possible to use. For information on the shape of the dark halo, which is presently unknown, it is important to observe microlensing in different directions. Two groups have started to perform searches: the French AGAPE (Andromeda Gravitational Amplification Pixel Experiment) [49] [50] and the American VATT/COLUMBIA [51] [52] which uses the 1.8-m VATT-telescope (Vatican Advanced Technology Telescope). Both teams showed that the pixel-lensing method works; however, the small number of observations so far does not allow the drawing of firm conclusions. Both the AGAPE and the VATT/COLUMBIA teams found some candidate events which are consistent with microlensing; however, additional observations are needed to confirm this.

[1] Current information on the MACHO collaboration's alert events is maintained at the WWW site http://darkstar.astro.washingtoisedu.

There are also networks involving different observatories with the aim of performing accurate photometry on alert microlensing events and in particular with the goal to find planets [53, 54, 55].

Although a rather young observational technique, microlensing has already enabled us to make substantial progress and the prospects for further contributions to solve important astrophysical problems look very bright.

Chapter 5

The lens equation in cosmology

Till now, we considered only almost static, weak localized perturbations of Minkowski spacetime. In cosmology the unperturbed spacetime background is given by a Robertson-Walker metric, and this induces various changes in the previous discussions. It turns out that the final result for the lens map and the time delay looks practically unchanged, essentially we only have to insert some obvious redshift factors and interpret all distances as *angular diameter distances*.

We recall that the expression for the time delay in an almost Newtonian situation is given by eq.(2.19) with eqs.(2.20), (2.21)

$$c\Delta t = \frac{D_d D_s}{2D_{ds}} \left(\frac{\vec{\xi}}{D_d} - \frac{\vec{\eta}}{D_s} \right)^2 - \hat{\psi}(\vec{\xi}) + const. \tag{5.1}$$

Notice that $\left(\frac{\vec{\xi}}{D_d} - \frac{\vec{\eta}}{D_s} \right) = (\vec{\theta} - \vec{\beta})$. If the distances involved are cosmological, we must multiply the whole expression by $(1 + z_d)$, where z_d is the redshift of the lens. In addition all distances must be interpreted as angular diameter distances. (For a detailed derivation we refer to the book of Schneider et al. [4] or [56]). With these modifications we get for the time delay

$$c\Delta t = (1 + z_d) \left[\frac{D_d D_s}{2D_{ds}} (\vec{\theta} - \vec{\beta}\,)^2 - \hat{\Psi}(\vec{\xi}\,) \right] + const. \,, \tag{5.2}$$

where the prefactor of the first term is proportional to $1/H_0$ (H_0 is the present Hubble parameter).

For cosmological applications, it is convenient to rewrite the potential term using the length scale $\xi_0 = D_d$ as defined in eq.(2.18) and $\vec{\theta} = \vec{\xi}/D_d$. This way we get

$$\hat{\psi}(\vec{\xi}) = \frac{4G}{c^2} \int d^2\theta' D_d^2 \Sigma(D_d \vec{\theta'}) \ln |\vec{\theta} - \vec{\theta'}| = 2R_s \tilde{\psi}(\vec{\theta}) \,, \tag{5.3}$$

where $R_s = 2GM/c^2$ is the Schwarzschild radius of the total mass M of the lens, and

$$\tilde{\psi}(\vec{\theta}) = \int d^2\theta' \tilde{\Sigma}(\vec{\theta}') \ln|\vec{\theta} - \vec{\theta}'| \ , \tag{5.4}$$

with

$$\tilde{\Sigma}(\vec{\theta}) := \frac{\Sigma(D_d\vec{\theta})}{M} D_d^2 \ . \tag{5.5}$$

This quantity gives the fraction of the total mass M per unit solid angle as seen by the observer. We can now write eq. (5.2) in the form

$$c\Delta t = \hat{\phi}(\vec{\theta}, \vec{\beta}) + const. \ , \tag{5.6}$$

where $\hat{\phi}$ is the *cosmological Fermat potential*

$$\hat{\phi}(\vec{\theta}, \vec{\beta}) = \frac{1}{2}(1+z_d)\frac{D_d D_s}{D_{ds}}(\vec{\theta} - \vec{\beta})^2 - 2R_s(1+z_d)\tilde{\psi}(\vec{\theta}) \ . \tag{5.7}$$

For a Friedmann–Lemaitre model with density parameter Ω_0 and vanishing cosmological constant Λ, the angular diameter distance $D(z_1, z_2)$ between two events at red shifts z_1 and z_2 $(z_1 < z_2)$, is given by

$$D(z_1, z_2) = 2c\frac{\sqrt{1+\Omega_0 z_1}(2 - \Omega_0 + \Omega_0 z_2) - \sqrt{1+\Omega_0 z_2}(2 - \Omega_0 + \Omega_0 z_1)}{H_0\Omega_0^2(1+z_2)^2(1+z_1)} \ . \tag{5.8}$$

Eqs.(5.6)-(5.7) provide the basis for the determination of the Hubble parameter with gravitational lensing. One should also take into account that the Universe might have a clumpy structure, which affects than the light propagation (for details on this problem see [57], [58]).

From eq.(5.7) we obtain the cosmological lens mapping using Fermat's principle, which implies that $\nabla_{\vec{\theta}}\hat{\phi}(\vec{\theta}, \vec{\beta}) = 0$ and gives an equation identical to eq.(2.22), but with the present meaning of the symbols it holds for arbitrary redshifts.

Consider two images at the (observed) positions $\vec{\theta}_1$, $\vec{\theta}_2$, with separation $\vec{\theta}_{12} \equiv \vec{\theta}_1 - \vec{\theta}_2$ and time delay Δt_{12}. Using the lens equation we obtain

$$\vec{\theta}_{12} = 2R_s\frac{D_{ds}}{D_d D_s}\left[\left.\frac{\partial\tilde{\psi}}{\partial\vec{\theta}}\right|_{\vec{\theta}_1} - \left.\frac{\partial\tilde{\psi}}{\partial\vec{\theta}}\right|_{\vec{\theta}_2}\right] \ . \tag{5.9}$$

The time delay $\Delta t_{12} = \hat{\phi}(\vec{\theta}_1, \vec{\beta}) - \hat{\phi}(\vec{\theta}_2, \vec{\beta})$ contains the unobservable angle $\vec{\beta}$, but this can be eliminated with the lens equation and eq.(5.9):

$$\Delta t_{12} = 2R_s(1+z_d)\left\{\frac{1}{2}\left(\left.\frac{\partial\tilde{\psi}}{\partial\vec{\theta}}\right|_{\vec{\theta}_1} + \left.\frac{\partial\tilde{\psi}}{\partial\vec{\theta}}\right|_{\vec{\theta}_2}\right)\cdot\vec{\theta}_{12} - \left(\tilde{\psi}(\vec{\theta}_1) - \tilde{\psi}(\vec{\theta}_2)\right)\right\} \ . \tag{5.10}$$

Given a lens model (i.e. $\tilde{\Sigma}(\vec{\theta})$), then eqs. (5.9) and (5.10) give a relation between the observables $\vec{\theta}_{12}$, Δt_{12} and H_0, provided that Ω_0, z_d, z_s are also known. Fortunately, the dependence on Ω_0 is in practice not strong.

Consider as an example a point source lensed by a point mass (Schwarzschild lens). Then $\tilde{\psi}(\vec{\theta}) = \ln|\vec{\theta}|$ and eq.(5.9) gives

$$\theta_{12} = 2R_s \frac{D_{ds}}{D_d D_s} \left(\frac{1}{\theta_1} - \frac{1}{\theta_2} \right) , \tag{5.11}$$

On the other hand, equation (5.10) becomes

$$\Delta t_{12} = 2R_s(1+z_d) \left\{ \frac{\theta_2^2 - \theta_1^2}{2|\theta_1\theta_2|} + \ln \left| \frac{\theta_2}{\theta_1} \right| \right\} . \tag{5.12}$$

We write this in terms of the ratio ν of the magnifications. Using eq.(3.24) one finds $\nu = \ln(\theta_2/\theta_1)^2$ and thus

$$\Delta t_{12} = R_s(1+z_d)\{\nu^{1/2} - \nu^{-1/2} + \ln\nu\} . \tag{5.13}$$

5.1 Hubble constant from time delays

As first noted by Refsdal in 1964 [59], time delay measurements can yield, in principle, the Hubble parameter. Unfortunately, the use of this method requires a reliable lens model. This introduces systematic uncertainties. Moreover, the cosmological Fermat potential involves the density parameter Ω_0 and Λ (set equal to zero in eq.(5.8)). The dependence on Ω_0 and Λ is, however, not strong, at least in some redshift domains ($z_s \leq 2, z_d \leq 0.5$).

Measuring the time delay is not an easy task as the history of the famous double QSO0957+561 demonstrates. Fortunately, the time delay for QSO0957+561 is now well known: $\Delta t = 417 \pm 3$ days [60]. Modelings lead to a best estimate of $H_0 \simeq 61$ km s^{-1} Mpc^{-1}. For this example there are constraints for modeling the lens, nevertheless it is difficult to assess an error for the value of H_0.

Another example is the Einstein ring system B0218+357. A single galaxy is responsible for the small image splitting of 0.3". The time delay was reported to be 12 ± 3 days and the value $H_0 \sim 70$ km s^{-1} Mpc^{-1} was deduced. The ongoing surveys will hopefully find new lenses that possess the desirable characteristics for a reliable determination of H_0.

Besides having the above mentioned problems, the determination of H_0 through gravitational lensing offers also some advantages as compared to the other methods. It can be directly used for large redshifts (~ 0.5) and it is independent of any other method. Moreover, it is based on fundamental physics, while other methods rely on models for variable stars (Cepheids), or supernova explosions (type II), or empirical calibrations of standard candles (Tully–Fisher distances, type I supernovae).

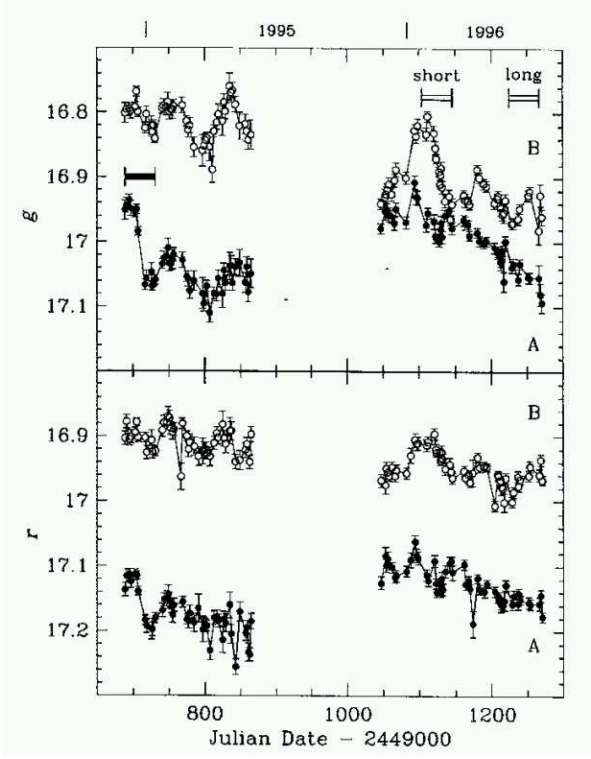

Figure 5.1. Lightcurves of the two images of the gravitationally lensed quasar Q0957+561. Note the sudden decrease of image A at the beginning of the 1995 season (taken from T. Kundić et al., 1997 [60]).

Finally, we notice that lensing can also lead to bounds on the cosmological constant. The volume per unit redshift of the universe at high redshifts increases for a large Λ. This implies that the relative number of lensed sources for a given comoving number density of galaxies increases rapidly with Λ. This can be used to constrain Λ by making use of the observed probability of lensing. Various authors have used this method and came up with a limit $\Omega_\Lambda \leq 0.6$ for a universe with $\Omega_0 + \Omega_\Lambda = 1$. It remains to be seen whether such bounds, based on lensing statistics, can be improved.

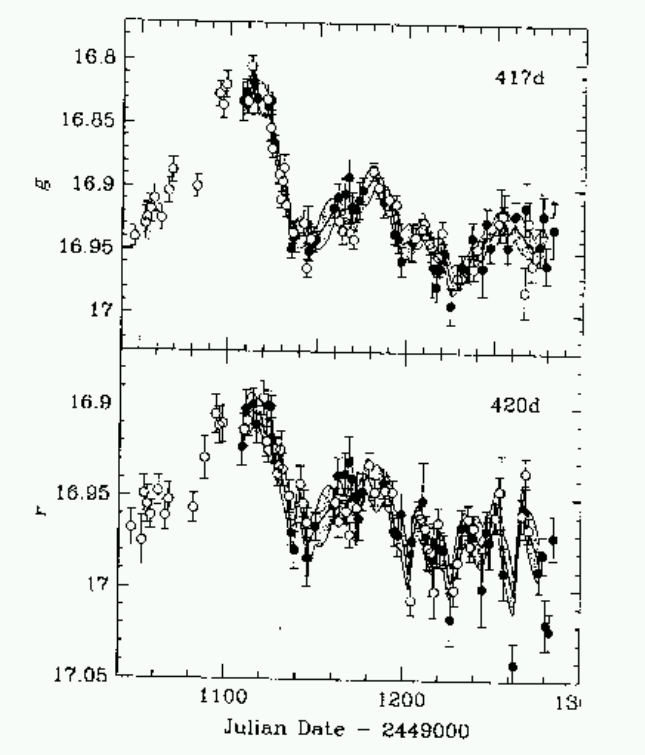

Figure 5.2. The lightcurve of image A of Fig. 4.1 is advanced by the optimal value of the time delay, 417 days (taken from T. Kundić et al., 1997 [60]).

Chapter 6

Galaxy clusters as lenses

Galaxy clusters similarly to galaxies can act as gravitational lenses for more distant galaxies. One classifies the observed lensing effects due to clusters into two types.

1) Rich centrally condensed clusters produce sometimes giant arc when a background galaxy turns out to be almost aligned with one of the cluster caustics (*strong lensing*). (See, for instance, Fig. 1.1.)

2) Every cluster produces weakly distorted images of a large number of background galaxies (*weak lensing*). A nice example is in Fig. 6.2.

Both these cases have been observed and allow to get important information on the distribution of the matter in galaxy clusters. For the analysis of giant arcs, we have to use parametrized lens models which are fitted to the observational data. The situation is much better for weak lensing, because there now exist several parameter–free reconstruction methods of projected mass distributions from weak lensing data.

Strong lensing requires that the mass density per surface Σ has to be in some parts of the lens bigger than the critical mass density given by

$$\Sigma \geq \Sigma_{crit} = \frac{c^2 D_s}{4\pi G D_d D_{ds}} \ . \tag{6.1}$$

Indeed, if this condition is satisfied there will be one or more caustics. The observation of an arc in a cluster of galaxies allows to easily estimate the projected cluster mass which lies inside a circle traced by the arc, even if no ring-shaped image is produced. For an axisymmetric lens, the average surface mass density within the tangential critical curve is given by Σ_{crit}. Tangentially oriented large arcs occur nearby the tangential critical curves, and thus the radius θ_{arc} of the circle traced by the arc gives an estimate of the Einstein radius θ_E. Inside the so defined circle the surface mass is Σ_{crit}, and this way, knowing the redshifts of the lens and the source, one

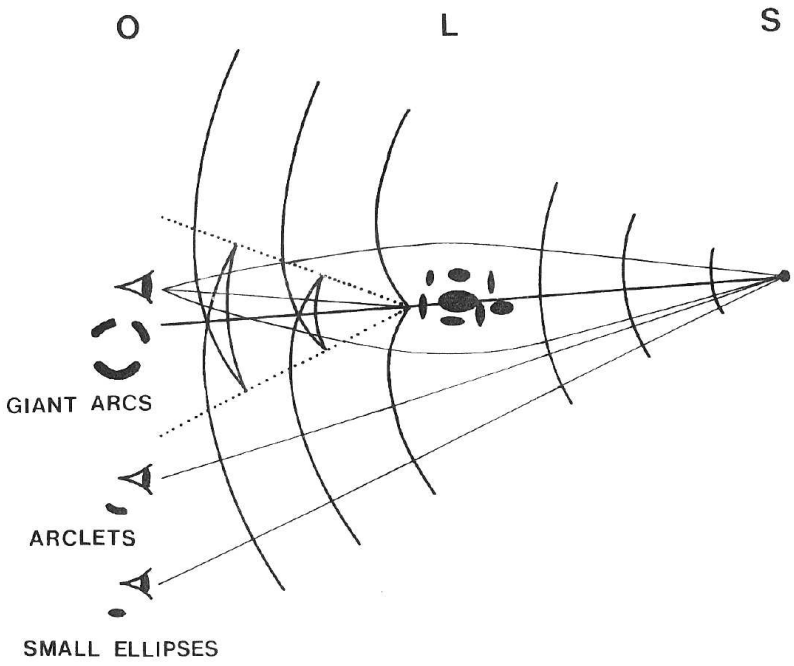

Figure 6.1. Wave fronts in the presence of a cluster perturbation.

finds the total mass enclosed by $\theta = \theta_{arc}$

$$M(<\theta) = \Sigma_{crit}\ \pi\ (D_d\ \theta)^2 \simeq 1.1 \times 10^{14} M_\odot \left(\frac{\theta}{30''}\right)^2 \left(\frac{D_d}{1Gpc}\right)\ , \quad (6.2)$$

A mass estimate with this procedure is useful and often quite accurate.

If we assume that the cluster can be at least as a first approximation be described as a singular isothermal sphere, then using eq. (3.34) we obtain for the dispersion velocity in the cluster

$$\sigma_v \simeq 10^3\ \mathrm{km/s} \left(\frac{\theta}{28''}\right)^{1/2} \left(\frac{D_s}{D_{ds}}\right)^{1/2}\ . \quad (6.3)$$

A limitation of strong lensing is that it is model dependent and moreover one can determine only the mass inside a cylinder of the inner part of a lensing cluster. The fact that the observed giant arcs never have counter-arc of comparable brightness, and rarely even small counter-arcs, implies that the lensing geometry has to be non-spherical.

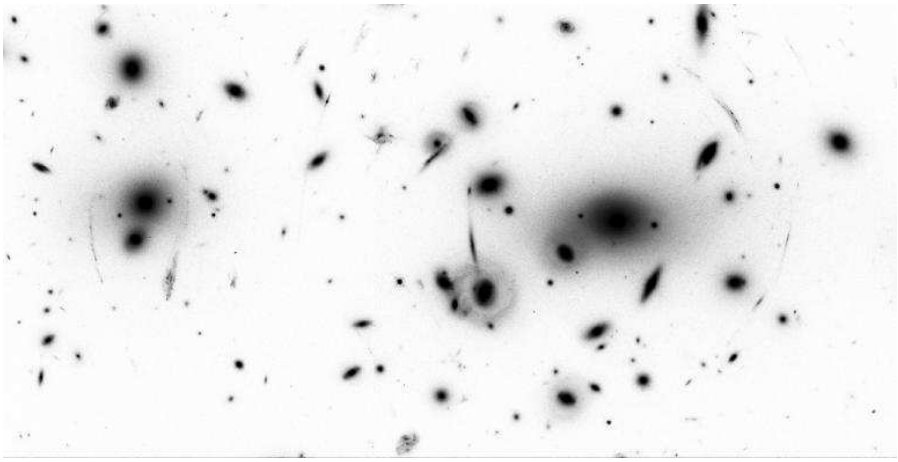

Figure 6.2. Hubble Space Telescope image of the cluster Abell 2218. Beside arcs around the two centers of the cluster, many arclets can be seen (NASA HST Archive).

A remarkable phenomenon is the occurrence of so–called *radial arcs* in galaxy clusters. These are *radially* rather than tangentially elongated, as most luminous arcs are. They are much less numerous (examples: MS 2137, Abell 370). Their position has been interpreted in terms of the turnover of the mass profile and a core radius $\sim 20\ h^{-1}$ kpc has been deduced, quite independent of any details of the lens model. There are, however, other mass profiles which can produce radial arcs, and have no flat core; even singular density profiles can explain radial arcs [61]. Such singular profiles of the dark matter are consistent with the large core radii inferred from X–ray emission.

6.1 Weak lensing

There is a population of distant blue galaxies in the universe whose spatial density reaches 50–100 galaxies per square arc minute at faint magnitudes. The images of these distant galaxies are coherently distorted by any foreground cluster of galaxies. Since they cover the sky so densely, the distortions can be determined statistically (individual weak distortions cannot be determined, since galaxies are not intrinsically round). Typical separations between arclets are $\sim (5-10)''$ and this is much smaller than the scale over which the gravitational cluster potential changes appreciably.

Starting with a paper by Kaiser and Squires [62], a considerable amount of theoretical work on various parameter-free reconstruction methods has

recently been carried out. The main problem consists in making an optimal use of limited noisy data, without modeling the lens. For reviews see [63, 64]. The derivation of most of the relevant equations gets much easier when using a complex formulation of lensing theory (see for instance [65]). In the following we will, however, not use it.

The reduced shear $\vec{g}$, introduced in Section 2.4, is in principle observable over a large region. What we are really interested in, however, is the mean curvature κ, which is related to the surface mass density. Since

$$\vec{g} = \frac{\vec{\gamma}}{1-\kappa} \tag{6.4}$$

we first look for relations between the shear $\vec{\gamma} = (\gamma_1, \gamma_2)$ and κ.

From equation (2.37) we get that

$$\Delta\Psi = 2k \tag{6.5}$$

or if instead we use the notation $\vec{\theta} = (\theta_1, \theta_2)$ for the image position eq.(6.5) can explicitely be written as

$$k(\vec{\theta}) = \frac{1}{2}\left(\frac{\partial^2\Psi(\vec{\theta})}{\partial\theta_1^2} + \frac{\partial^2\Psi(\vec{\theta})}{\partial\theta_2^2}\right) \ . \tag{6.6}$$

Using the definition for γ_i as given in eq.(2.42) we find

$$\gamma_1(\vec{\theta}) = \frac{1}{2}\left(\frac{\partial^2\Psi(\vec{\theta})}{\partial\theta_1^2} - \frac{\partial^2\Psi(\vec{\theta})}{\partial\theta_2^2}\right) \equiv D_1\Psi \tag{6.7}$$

and

$$\gamma_2(\vec{\theta}) = \frac{\partial^2\Psi(\vec{\theta})}{\partial\theta_1\partial\theta_2} \equiv D_2\Psi \ . \tag{6.8}$$

where

$$D_1 := \frac{1}{2}\left(\partial_1^2 - \partial_2^2\right) \ , \qquad D_2 := \partial_1\partial_2 \ . \tag{6.9}$$

Note the identity

$$D_1^2 + D_2^2 = \frac{1}{4}\Delta^2 \ . \tag{6.10}$$

Hence

$$\Delta\kappa = 2\sum_{i=1,2} D_i\gamma_i \ . \tag{6.11}$$

Here, we can substitute the reduced shear, given by eq.(6.4), on the right for γ_i. This gives the important equation

$$\Delta\kappa = 2\sum_i D_i[g_i\,(1-\kappa)] \ . \tag{6.12}$$

For a given (measured) $\vec{g}$ this equation does not determine uniquely κ, indeed eq. (6.12) remains invariant under the substitution

$$\kappa \to \lambda\kappa + (1-\lambda) \ , \tag{6.13}$$

where λ is a real constant. This is the so-called *mass–sheet degeneracy* (a homogeneous mass sheet does not produce any shear).

Eq. (6.12) can be turned into an integral equation, by making use of the fundamental solution

$$\mathcal{G} = \frac{1}{2\pi} \ln \mid \vec{\theta} \mid \ , \tag{6.14}$$

(see Section 2.4) for which $\Delta\mathcal{G} = \delta^2$ (δ^2 is the two-dimensional delta function). Then we get

$$k(\vec{\theta}) = 2 \int_{R^2} d^2\theta' \ \mathcal{G}(\vec{\theta} - \vec{\theta'}) \sum_{i=1,2} (D_i \gamma_i)(\vec{\theta'}) + k_0 \ . \tag{6.15}$$

After some manipulations we can bring eq.(6.15) into the following form

$$k(\vec{\theta}) = \frac{1}{\pi} \sum_{i=1,2} \int_{R^2} d^2\theta' \ \left[\tilde{\mathcal{D}}_i(\vec{\theta} - \vec{\theta'}) \gamma_i(\vec{\theta'}) \right] + k_0 \ , \tag{6.16}$$

or in terms of the reduced shear

$$k(\vec{\theta}) = k_0 + \frac{1}{\pi} \sum_{i=1,2} \int_{R^2} d^2\theta' \ \left[\tilde{\mathcal{D}}_i(\vec{\theta} - \vec{\theta'}) (g_i(1-k))(\vec{\theta'}) \right] \ , \tag{6.17}$$

where

$$D_1 \ln \mid \vec{\theta} \mid = \frac{\theta_2^2 - \theta_1^2}{\mid \vec{\theta} \mid^4} \equiv \tilde{\mathcal{D}}_1 \ , \qquad D_2 \ln \mid \vec{\theta} \mid = -\frac{2\theta_1\theta_2}{\mid \vec{\theta} \mid^4} \equiv \tilde{\mathcal{D}}_2 \ . \tag{6.18}$$

The crucial fact is that $\gamma(\vec{\theta})$ is an observable quantity and thus using eq.(6.16) one can infer the matter distribution of the considered galaxy cluster. This result is, however, fixed up to an overall constant k_0 (problem of the mass-sheet degeneracy).

As discussed in Section 2.4 we can define the ellipticity ϵ of an image of a galaxy as

$$\epsilon = \epsilon_1 + i\epsilon_2 = \frac{1-r}{1+r} e^{2i\varphi} \ , \quad r \equiv \frac{b}{a} \ , \tag{6.19}$$

where φ is the position angle of the ellipse and a and b are the major and minor semiaxis, respectively. a and b are given by the inverse of the eigenvalues of the matrix defined in eq. (2.42). If we take the average on

the ellipticity due to lensing and make use of eq.(6.19) as well as of the expressions for a and b we find the relation

$$< \epsilon > \;=\; \left\langle \frac{\gamma}{1-k} \right\rangle \;. \tag{6.20}$$

The angle bracket means average over a finite sky area. In the weak lensing limit $k \ll 1$ and $\mid \gamma \mid \ll 1$ the mean ellipticity directly relates to the shear: $< \gamma_1(\vec{\theta}) > \simeq < \epsilon_1(\vec{\theta}) >$ and $< \gamma_2(\vec{\theta}) > \simeq < \epsilon_2(\vec{\theta}) >$. Thus a measurement of the average ellipticity allows to determine γ, and making use of eq.(6.16) one can get the surface mass density k of the lens. Recently, several groups reported the detection of cosmic shear, which clearly demonstrates the technical feasibility of using weak lensing surweys to measure dark matter clustering and the potential for cosmological measurements, in particular with the upcoming wide field CCD cameras [67, 68].

6.2 Comparison with results from X–ray observations

Beside the lensing technique, there are two other methods for determining mass distributions of clusters:
1) The observed velocity dispersion, combined with the Jeans–equation from stellar dynamics gives the total mass distribution, if it is assumed that light traces mass.
2) X–ray observations of the intracluster gas, combined with the condition of hydrostatic equilibrium and spherical symmetry lead also to the total mass distribution as well as to the baryonic distribution.

If the hydrostatic equilibrium equation for the hot gas

$$\frac{dP_g}{dr} = -\rho_g \frac{GM_t\,(r)}{r^2} \tag{6.21}$$

is combined with the ideal equation of state $P_g = (k_B T_g/\mu m_H)\,\rho_g$ and assuming spherical symmetry, one easily finds for the total mass profile

$$M_t\,(r) = -\frac{k_B T_g}{G\mu m_H} \left(\frac{d\ln \rho_g}{d\ln r} + \frac{d\ln T_g}{d\ln r} \right) r. \tag{6.22}$$

The right hand side can be determined from the intensity distribution and some spectral information. (At present, the latter is not yet good enough, because of relatively poor resolution, which, however, will change with the XMM survey.)

Weak lensing together with an analysis of X–ray observations offers a unique possibility to probe the relative distributions of the gas and the dark matter, and to study the dynamical relationship between the two. As an example consider the cluster of galaxies A2163 (z=0.201) which is one of the two most massive clusters known so far.

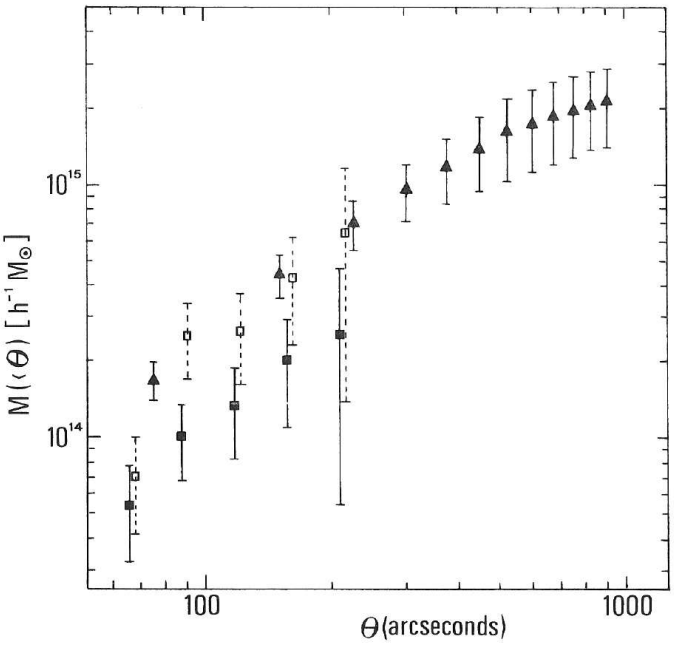

Figure 6.3. The radial mass profiles determined from the X–ray and lensing analysis for Abell 2163. The triangles display the total mass profile determined from the X–ray data. The solid squares are the weak lensing estimates "corrected" for the mean surface density in the control annulus determined from the X–ray data. The conversion from angular to physical units is $60'' = 0.127\ h^{-1}$ Mpc (taken from G. Squires et al., 1997 [66]).

ROSAT measurements reach out to 2.3 h^{-1} Mpc (~ 15 core radii)(h being the Hubble constant in units of 100). The total mass is 2.6 times greater than that of COMA, but the gas mass fraction, $\sim 0.1\ h^{-3/2}$ is typical for rich clusters. The data together suggest that there was a recent merger of two large clusters. The optical observations of the distorted images of background galaxies were made with the CFHT telescope. The resulting lensing and X–ray mass profiles are compared in Fig. 6.3. The data sets only overlap out to a radius of $200'' \simeq 500\ h^{-1}$ kpc to which the lensing studies were limited. It is evident that the lensing mass estimates are systematically lower by a factor of $\simeq 2$ than the X–ray results, but

generally the results are consistent with each other, given the substantial uncertainties. There are reasons that the lensing estimate may be biased downward. Correcting for this gives the results displayed by open squares. The agreement between the lensing and X–ray results becomes then quite impressive. The rate and quality of such data will increase dramatically during the coming years. With weak lensing one can also test the dynamical state of clusters. By selecting the relaxed ones one can then determine with some confidence the relative distributions of gas and dark matter.

In addition, it will become possible to extend the investigations to super clusters scales, with the aim to determine the power spectrum and get information on the cosmological parameters [63, 64].

References

[1] S. Perlmutter et al. (1999), Astrophys. J. **517** 565
[2] V. Trimble (1987), Annu. Rev. Astron. Astrophys. **25** 425
[3] F. Zwicky (1933), Helv. Phys. Acta **6** 110
[4] P. Schneider, J. Ehlers and E. E. Falco (1992), *Gravitational Lensing*. (Springer Verlag, Berlin 1992)
[5] S. Refsdal and J. Surdej (1994), *Gravitational lenses*. Rep. Prog. Phys. **56** 117
[6] R. Narayan and M. Bartelmann (1996), *Lectures on Gravitational Lensing*. astro-ph 9606001
[7] N. Straumann, Ph. Jetzer and J. Kaplan (1998), *Topics on Gravitational Lensing*. Napoli Series on Physics and Astrophysics (Bibliopolis, Naples)
[8] F. W. Dyson, A. S. Eddington and C. R. Davidson (1920), Mem. Royal Astronomical Society **62** 291
[9] A. Einstein (1936), Science **84** 506
[10] J. Renn, T. Sauer and J. Stachel (1997), Science **275** 184
[11] F. Zwicky (1937), Phys. Rev. **51** 290; (1937), Phys. Rev. **51** 679
[12] K. Chang and S. Refsdal (1979), Nature **282** 561
[13] R. J. Gott (1981), Astrophys. J. **243** 140
[14] B. Paczyński (1986), Astrophys. J. **301** 503
[15] R. Schmidt and J. Wambsganss (1998), Astron. and Astrophys. **335** 379
[16] J. Wambsganss (2000), astro-ph 0008419
[17] B. Paczyński (1986), Astrophys. J. **304** 1
[18] A. De Rújula, Ph. Jetzer and E. Massó (1991), Mont. Not. R. Astr. Soc. **250** 348
[19] A. De Rújula, Ph. Jetzer and E. Massó (1992), Astron. and Astrophys. **254** 99
[20] K. Griest (1991), Astrophys. J. **366** 412
[21] R. J. Nemiroff (1991), Astron. and Astrophys. **247** 73
[22] B. Paczyński (1996), Annu. Rev. Astron. Astrophys. **34** 419
[23] E. Roulet and S. Mollerach (1997), Phys. Rept. **279** 67
[24] A.F. Zakharov and M.V. Sazhin (1998), Physics Uspekhi **41** 945
[25] Ph. Jetzer (1999), Naturwissenschaften **86** 201
[26] B. Carr (1994), Annu. Rev. Astron. Astrophys. **32** 531
[27] J. Bahcall, C. Flynn, A. Gould and S. Kirhakos (1994), Astrophys. J. **435** L51
[28] E. J. Kerins (1997), Astron. and Astrophys. **322** 709

[29] G. Gilmore and M. Unavane (1998), Mont. Not. R. Astr. Soc. **301** 813
[30] C.M. Tamanaha, J. Silk, M.A. Wood and D.E. Winget (1990), Astrophys. J. **358** 164
[31] S.D. Kawaler (1996), Astrophys. J. **467** L61
[32] F. De Paolis, G. Ingrosso, Ph. Jetzer and M. Roncadelli (1995), Phys. Rev. Lett. **74** 14
[33] F. De Paolis, G. Ingrosso, Ph. Jetzer and M. Roncadelli (1995), Astron. and Astrophys. **295** 567
[34] F. De Paolis, G. Ingrosso, Ph. Jetzer and M. Roncadelli (1999), Astrophys. J. **510** L103
[35] B. Paczyński (1991), Astrophys. J. **371** L63
[36] K. Griest et al. (1991), Astrophys. J. **372** L79
[37] E. Aubourg et al. (1993), Nature **365** 623
[38] C. Alcock et al. (1993). Nature **365** 621; (1995), Astrophys. J. **445** 133
[39] C. Alcock et al. (2000), astro-ph 0001272
[40] C. Renault et al. (1997), Astron. and Astrophys. **324** L69
[41] C. Alcock et al. (1997), Astrophys. J. **491** L11
[42] N. Palanque-Delabrouille et al. (1999), Astron. and Astrophys. **332** 1
[43] C. Alcock et al. (1997), Astrophys. J. **479** 119
[44] A. Udalski et al. (1994), Acta Astron. **44** 165
[45] L. Grenacher, Ph. Jetzer, M. Strässle and F. De Paolis (1999), Astron. and Astrophys. **351** 775
[46] A.P. Crotts (1992), Astrophys. J. **399** L43
[47] P. Baillon, A. Bouquet, Y. Giraud-Héraud and J. Kaplan (1993), Astron. and Astrophys. **277** 1
[48] Ph. Jetzer (1994), Astron. and Astrophys. **286** 426
[49] R. Ansari et al. (1997), Astron. and Astrophys. **324** 843.
[50] R. Ansari et al. (1999), Astron. and Astrophys. **344** L49
[51] A.P.S. Crotts and A.B. Tomaney (1996), Astrophys. J. **473** L87,
[52] A. Crotts and R. Uglesich (2000), astro-ph 0006282
[53] S. Mao and B. Paczyński (1991), Astrophys. J. **374** L37
[54] A. Gould and A. Loeb (1992), Astrophys. J. **396** 104
[55] D. Bennett and S.H. Rhie (1996), Astrophys. J. **472** 660
[56] N. Straumann (1999), *Lectures on Gravitational Lensing*. Troisième Cycle de la Physique en Suisse Romande
[57] R.K. Sachs (1961), Proc. Roy. Soc. London **A264** 309
[58] C.C. Dyer and R.C. Roeder (1973), Astrophys. J. **180** L31
[59] S. Refsdal (1966), Mont. Not. R. Astr. Soc. **134** 315
[60] T. Kundić et al. (1997), Astrophys. J. **482** 648
[61] M. Bartelmann (1996), Astron. and Astrophys. **313** 697
[62] N. Kaiser and G. Squires (1993), Astrophys. J. **404** 441
[63] Y. Mellier (1999), Annu. Rev. Astron. Astrophys. **37** 127
[64] M. Bartelmann and P. Schneider (1999), *Weak Gravitational Lensing*. astro-ph 9912508
[65] N. Straumann (1997), Helv. Phys. Acta **70** 894
[66] G. Squires et al. (1997), Astrophys. J. **482** 648
[67] L. Van Waerbeke et al. (2000), astro-ph 0002500
[68] D.M. Wittman et al. (2000), astro-ph 0003014

Index

arrival time, 10
axial symmetry, 19
axially symmetric, 16

caustics, 12
cold clouds, 26
cosmology, 35
critical curves, 17
critical points, 12

deflection angle, 6, 7

Einstein, 2, 3
Einstein radius, 18, 19, 22, 40

Fermat potential, 10, 12, 17, 36
Fermat principle, 9, 10

galaxy clusters, 40
general relativity, 2
giant arcs, 41
gravitational lens, 8, 40
gravitational lensing, 1, 2

hydrogen gas, 26

isothermal sphere, 21

Jacobi matrix, 12, 17

lens equation, 9, 11, 12, 17
lens mapping, 12, 36
lens plane, 7, 12

MACHO, 25–32
microlensing, 20, 25, 28, 30, 31, 33, 34

Newton, 3

optical depth, 28, 29

point-like lens, 6

reduced shear, 13, 43
refraction index, 5

Schwarzschild lens, 19, 20, 27
Schwarzschild radius, 7
Soldner, 3
source plane, 7
speed of light, 6

time delay, 6, 35, 37

weak lensing, 40, 45, 47

Zwicky, 1, 3